FOREWORD

The research work described in this report was performed by the Bell Aerosystems Company, Buffalo, New York, for the Flight Dynamics Laboratory, Research and Technology Division, Wright-Patterson Air Force Base, Ohio. The work was accomplished under Contract No. AF33(657)-7486, Project No. 8219, Task No. 821901, and entitled "Nonlinear Thermoelastic Effects on Hypersonic Stability and Control"; Mr. H.M. Davis and Mr. J.E. Jenkins have been the Air Force Project Officers since the initiation of the program in November 1961. The study program was carried out by the Vehicle Structures Department of Bell Aerosystems Company under the Technical Direction of Mr. V.W. Donato and Mr. J.R. Batt.

A portion of the results of this program are being presented in a two-part report, under report number FDL TDR 64-16. Part I presents a method for obtaining hypersonic aerodynamic influence coefficient matrices. In Part II, a method is presented for obtaining hypersonic static aerothermoelastic solutions in the presence of nonlinear aerodynamic and structural behavoir and includes data from tests simulating this behavior. A computer program for the solution of non-linear static aerothermoelastic problems is also presented. This program is available to eligible recipients from the Control Criteria Branch, Flight Control Division, Flight Dynamics Laboratory, Wright Patterson AFB, Ohio. The work described in this report is being published under separate cover.

Acknowledgments are given to Mr. D.J. Haag for his assistance in the tedious reduction and presentation of test results, to Mr. E. Stanton for providing the necessary photography, and to Mr. D. Powers for his assistance in the preparation of the mirrored surfaces.

ABSTRACT

Results of a study of the feasibility of employing the Moire' fringe technique in the measurement of angular displacements of practical wing structures are presented. Slope influence coefficients obtained from Moire' fringe patterns determined from a square cantilever plate and a swept wing model are compared with available theoretical and experimental data.

This Technical Documentary report has been reviewed and is approved.

C R Bryan

for W. A. SLOAN, Jr.
Colonel, USAF
Chief, Flight Control Division
AF Flight Dynamics Laboratory

Contrails

TABLE OF CONTENTS

ILLUSTRATIONS

ILLUSTRATIONS (CONT)

SECTION 1.0

INTRODUCTION

The analysis of the static aeroelastic behavior of lifting surfaces requires a knowledge of the streamwise slope influence coefficients. As analytical methods have become more refined and the actual structures more complex, the trend in idealization has been towards the use of greater numbers of points for which such influence coefficients must be defined. The ultimate objective of this trend can be regarded as a representation for which the slope influence coefficients are known at every point on the surface. Sophisticated analysis techniques (e.g., matrix structural analysis) cannot as yet provide a representation to this degree of refinement. Certain experimental techniques, however, are extremely promising in this regard. The feasibility of employing one such experimental technique - the Moire' fringe method - for the evaluation of the slope influence coefficients of practical lifting surface structures is examined in this report.

The Moire' fringe method, as employed here, is a photographic technique in which a gridwork of lines is reflected from a deflected reflective surface and the surface is photographed, in double exposure, at two successive deflection levels. The developed photograph will contain a series of lines, or "fringes", each representing a line of constant slope in a given direction as produced by the change in load between the successive levels. The technique thereby establishes the change in slope in the given direction at each point of the surface. The required equipment is relatively inexpensive and simple to operate.

The Moire'fringe technique was originated as an experimental method for the determination of the stresses in laterally loaded thin flat plates (References 1-3). The stresses are obtained by computational operations on the directly measured slopes. Ligtenberg (Reference 1) devised the fixtures and test procedures which have found application in the more recent studies, including the present study, and is responsible for the concept of utilizing a double exposure in taking the required

1

photographs. One of the most extensive series of plate tests was performed by Bradley (Reference 2), who presents information on various schemes for making reflective the surfaces tested.

The subject applications (lifting surfaces of built-up aluminum alloy construction) differ from those already described in the literature in the following significant respects:

(1) The surface of a practical wing possesses geometric irregularities resulting from riveting and sheet metal working operations.

(2) The surface of a practical wing is nonplanar, i.e., it is tapered or curved in both directions.

(3) The material of construction is, in general, not amenable to direct operations which will render it reflective to the required degree.

(4) The lifting surfaces of practical airframes are, to an order of magnitude, larger than flat plate specimens tested in previously published studies.

Thus, the present study has concentrated attention on the above problem areas, with preliminary operations devoted to the duplication of the simple flat plate experiments conducted elsewhere. In examining the above special problems, tests were performed on a multiweb aluminum alloy wing model. This model had already been the subject of extensive analyses and tests for linear displacement (deflectional) influence coefficients and therefore provided an excellent basis for theory test comparisons.

Section 2 of this report describes the test apparatus developed for performance of the planned experiments. Then, in Section 3 the test specimens and techniques for establishing a reflective surface upon the specimens are described. The test procedures and results are also given in Section 3. The results are compared with alternate analytical and experimental data in Section 4. It is concluded that the subject technique is indeed practical and has considerable promise for the intended purposes, even in the presence of thermal and large deflection effects. Further developmental work is required, however, with respect to surface preparation techniques and still other matters. The conclusions and recommendations are detailed in Section 5.

SECTION 2.0

TEST APPARATUS

2.1   GENERAL CONCEPTS OF THE MOIRE' FRINGE TECHNIQUE

Before a description is given of the development of the various component elements of the test setup, it is necessary to outline the concepts underlying the Moire'technique. With this information, the functions to be performed by the respective components and the design basis of these components can be understood.

The Moire'technique for the direct determination of slope is based on an optical phenomenon revealed in the form of "fringes" which are produced when two sets of parallel lines are superimposed and one set is rotated with respect to the other so that the two sets intersect. Figure 2.1 shows a set of parallel equally spaced black and white lines. When two such sets are superimposed and one set is rotated with respect to the other, Moire'fringes appear as shown in Figure 2.2. These fringes are exhibited as a result of the concentration of light and dark areas (Figure 2.3) which essentially locates the regions or points of intersection of the two sets of black and white lines. As demonstrated in Reference 4, fringe patterns, of this type can be employed to determine the relative angular inplane position of one set of lines with respect to the other by a simple relationship between the grid line spacing, distance between fringes and angle of rotation.

A more distinct definition of the fringes is obtained by use of a simple photographic superposition technique which makes use of only one set of grid lines.   The technique consists of first photographing the set of lines in its initial position. After rotating the grid while holding the camera stationary, a second exposure is taken on the same film. Two superimposed sets of lines will then appear on the negative as shown in Figure 2.2. The white lines in this figure correspond to the white lines of the grid. A print of this negative produces a
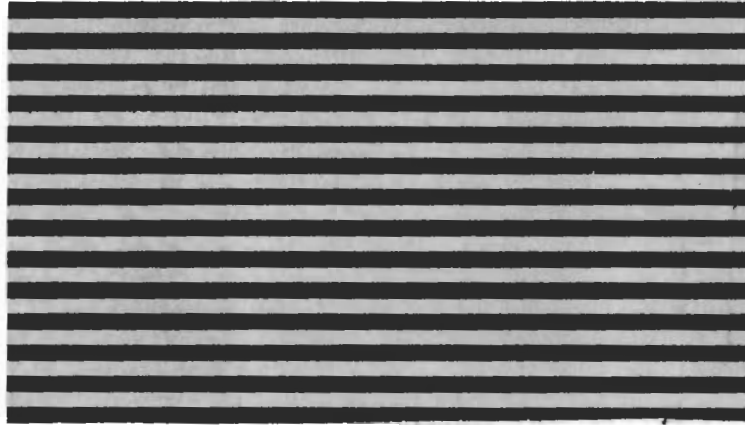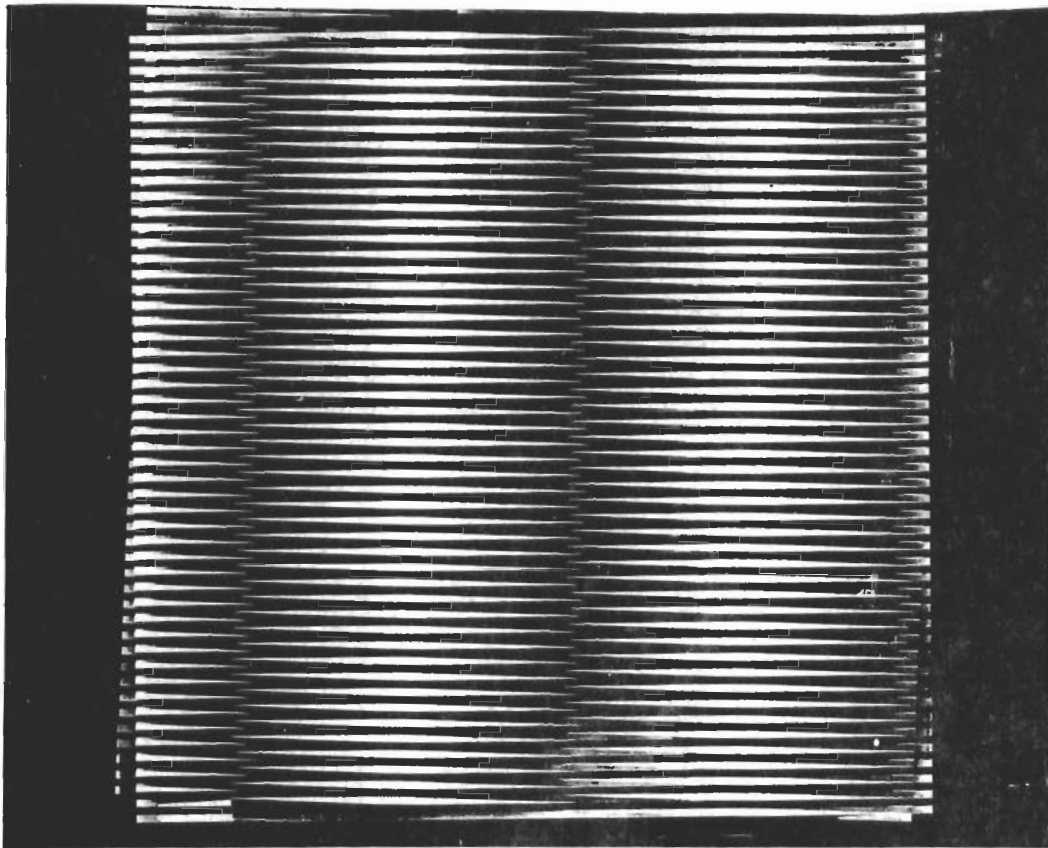
3

Figure 2.1. Parallel Black and Light Grid Lines

Figure 2.2. Negative of a Photograph of Two Sets of Superimposed Grid Lines

4
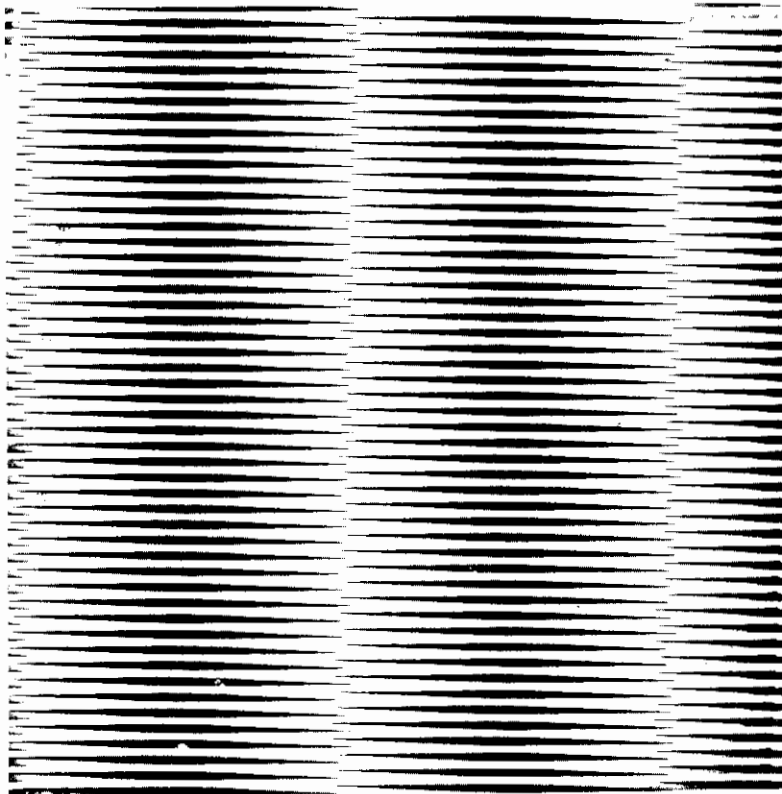
Figure 2.3. Detail of Moire' Fringes

distinct pattern of dark and light fringes as shown in Figure 2.3. The dark fringes correspond to only that portion of the superimposed black grid lines which over-lapped, i.e., the region where the black grid lines crossed. When the grid line spacing is sufficiently small, a relatively continuous set of well defined dark fringes will appear with a distinctness dependent to a large extent on the photographic equipment and procedure employed.

The manner in which the above concept is utilized in slope determinations for laterally loaded planar surfaces is illustrated in Figure 2.4. A cylindrical screen with a grid of equally spaced parallel black and white lines on its surface and parallel to the generatrix of the cylinder is placed in front of the reflective (mirrored) surface of the test specimen. A camera is positioned behind a small hole in the screen. The screen is illuminated by lights placed behind the specimen. Thus, the camera views the grid of the screen by reflection from the model surface.

At the beginning of a test, with either zero load or a specified load, a photograph is taken of the reflected gridwork. The film is exposed, the load is changed, and another photograph is taken of the reflected gridwork, using the same photographic plate.

The first exposure of the film will result in only a reproduction of the reflected grid contained within the confines of the mirrored test specimen surface. This exposure will reveal the outer contour of the mirrored surface and the specimen support edges. Grid lines recorded on the film during this step are essentially reference lines which properly orient the fringe patterns to the plate. Hence, as indicated in Figure 2.4, the grid line denoted by M on the screen will be reflected at point L on the mirrored surface of the specimen to point I on the film.

Deflection of the specimen by the application of a load will result in the distortion of the reflected grid lines which are photographed during the second exposure. As a consequence of this distortion, the two sets of superimposed lines will cross each other and thereby produce fringes.

Once the fringe pattern is obtained, it is next necessary to assign a slope magnitude to each fringe. This aspect of the method will now be discussed.
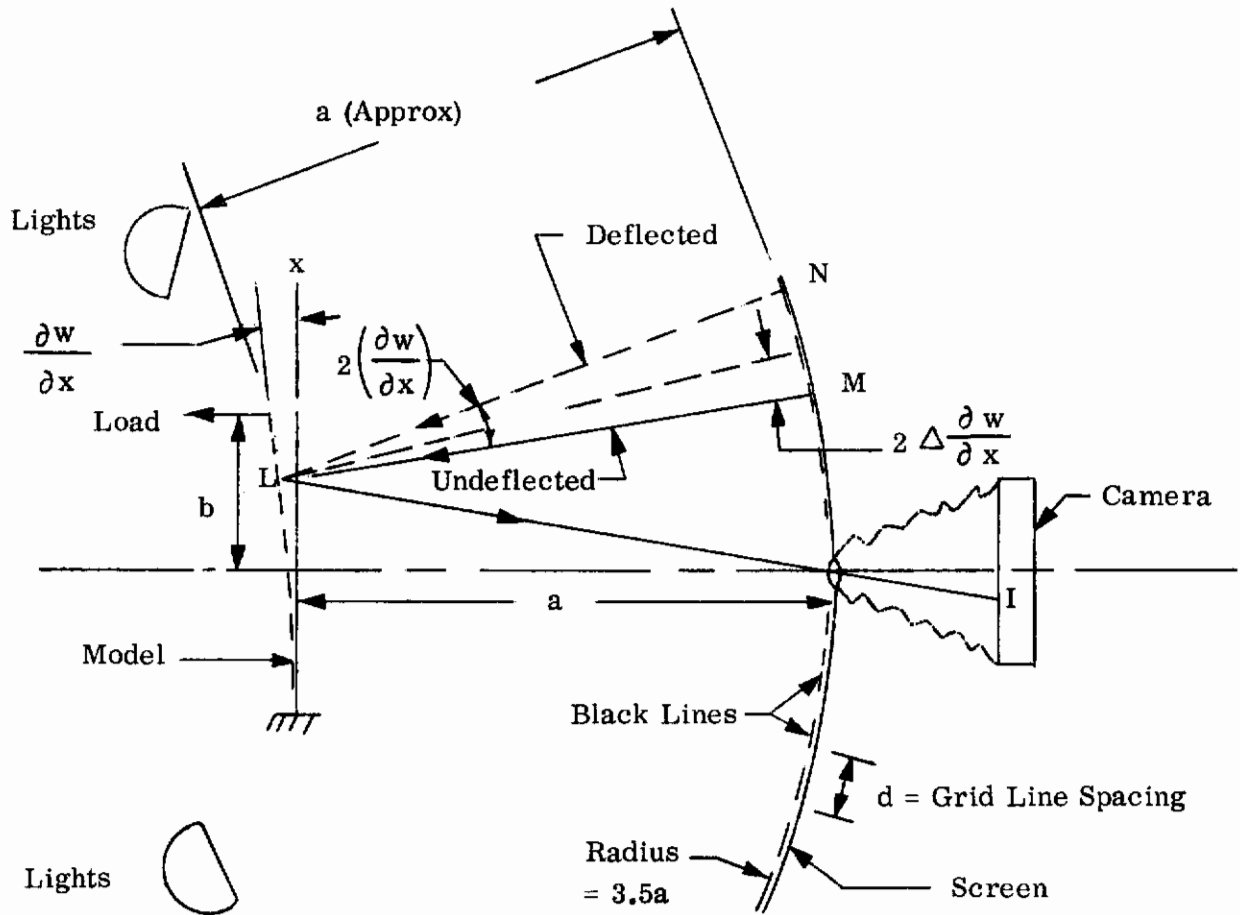
6

Figure 2.4. Schematic of Test Arrangement Top View

7

In general, a fringe will occur at point I on the screen (corresponding to point L on the mirrored surface) when the image at point L is a dark line. This will occur when, as a consequence of specimen deflection, point N appears instead of point M, where the distance NM is a multiple of d, the grid line spacing. From an inspection of the geometric arrangement of the screen test surface and camera, it is seen that for small deflections, w, the total angular deflection, $\frac{\partial w}{\partial x}$, at point L on the specimen is given by the following relation.

$$\frac{\partial w}{\partial x} = \frac{\overline{NM}}{2a} \tag{2.1}$$

Where $\overline{NM}$ equals the distance from point N to M on the screen and "a" is the distance of the camera to the mirrored surface. In the derivation of (2.1) it was assumed that the distances $\overline{LM}$ and $\overline{LN}$ are approximately equal to "a", a constant.

Since the distance $\overline{NM}$ is a multiple of d, Equation 2.1 can be written as

$$\frac{\partial w}{\partial x} = \frac{nd}{2a} \tag{2.2}$$

where $n = \overline{NM}/d$. It follows from Equation (2.2) that the change in slope corresponding to a distance of d on the screen will be

$$\Delta \frac{\partial w}{\partial x} = \frac{d}{2a} \tag{2.3}$$

where

$$\Delta \frac{\partial w}{\partial x} = \frac{1}{n} \frac{\partial w}{\partial x}$$

From the above development it is evident that each fringe represents a contour of constant slope about a line parallel to the grid lines and that the angular change between fringes is given by Equation (2.3). In addition, angular deflections can be obtained in any desired direction by proper orientation of the grid lines.

A desirable feature of this approach is that slope changes can be obtained even in the presence of the initial slopes which prevail in practical structures. Large initial slopes will require additional consideration, however, because the assumption that the radial dimension "a" is approximately constant may be significantly violated.

8

The change in slope between fringes is given by Equation (2.3) which is used to determine the corresponding slope magnitude for each fringe. This determination can be readily accomplished by a knowledge of the slopes at the boundary or supports of the specimen. Thus, at a fixed edge where the slope is zero a dark fringe, representing a zero slope condition, will always appear. Consequently, the first dark fringe from the boundary will represent a slope of magnitude $\Delta\dfrac{\partial w}{\partial x} = \dfrac{d}{2a}$ which is equal to the change of slope between fringes. It follows that for the nth dark fringe from the boundary there will be n equal changes of slope and therefore the related total slope will be $\dfrac{\partial w}{\partial x} = n\ \Delta\dfrac{\partial w}{\partial x} = \dfrac{nd}{2d}$.

From experiences with Moire' fringe patterns it has been generally found that the light fringes were more distinct than the dark fringes. For such situations the light fringes can be readily used to obtain the slopes by noting that the first light fringe from a fixed edge of zero slope corresponds to an angle change of $\dfrac{1}{2}\ \Delta\ \dfrac{\partial w}{\partial x}$. Hence, the slope at the nth light fringe from this fixed edge is

$$\frac{\partial w}{\partial x} = \frac{1}{2}\ \Delta\frac{\partial w}{\partial x} + (n-1)\ \Delta\frac{\partial w}{\partial x} \tag{2.4}$$

and, after noting Equation (2.3), reduces to

$$\frac{\partial w}{\partial x} = (n-\frac{1}{2})\frac{d}{2a} \tag{2.5}$$

2.2 RULED SCREEN

An overall view of the setup for tests performed at Bell Aerosystems Company is given in Figures 2.5 and 2.6. Basically, the screen is plywood with the ruled lines being drawn on sheets which are affixed to the plywood surface.

The size of the structures to be tested required that the field of view (b) be 16 inches. Using the expressions $b = 0.4a$ and $R = 3.5a$, as recommended in Reference 1, the radius of the screen was chosen as $R = 140.0$ in. and the distance from the center of the screen to the reflective surface of the test specimens as $a = 40.0$ in. Reference 1 also recommends that the width of the white and black

9

lines $(\frac{d}{2})$ be determined as $\frac{d}{2}$ = 0.002a = 0.08 in. Since, however, the present test

setup is relatively large it was felt desirable, from a photographic aspect, to

utilize a larger line width of 0.16 inches which corresponds to an angle change

$\Delta \frac{\partial w}{\partial x}$ = 0.004 rad instead of the 0.002 rad recommended. However, it was found that the

larger line width did not yield sufficiently high densities of fringes for the deflect-

ions that could be obtained from the specimens of interest. Consequently, the latter

portions of the tests were performed with the smaller recommended line width.

One of the major difficulties in constructing the desired apparatus stem-

med from the requirement that lines mounted on the screen be accurate with respect

to both width and parallelism. Various schemes for providing these lines were

examined, including a direct drawing of the lines on the screen and the cementing

of black strips of tape to the screen. After exploring these and other methods it was

found that the most satisfactory procedure was to print adhesive backed sheets, 8

inches square, with the desired lines and attach these sheets to the screen. The

sheets were printed from a plate obtained from a photograph of a white metal sheet

with properly spaced strips of black tape cemented to it. The spacings of the tape

were carefully checked with optical instruments.

The ruled sheets were attached to the screen only where required. Be-

cause of the size of the screen, small errors were introduced in the parallelism of

the lines from sheet to sheet. An experimental check of these errors showed that

they were indeed negligible. Another source of error relating to the ruled screen

arose during the experiments, when the cemented sheets tended to wrinkle and

expand or shrink as a result of changing humidity and temperatures.

A hole was placed in the screen at its center through which the camera

could view the specimen. For the relatively small specimens and the larger grid

line width, which required a larger distance between specimen and screen, a hole

diameter of 1/4 inch was sufficient. However, for the larger specimens and smaller

grid lines it was found necessary to enlarge the hole and to bevel its edge to pre-

vent interference with the camera field of view. It was found that hole size had no

significant effect on the results.

10

2.3   PHOTOGRAPHIC DEVICES

The screen was illuminated by two banks of lights (one bank to each side of the test specimen). These banks contained ten 150 watt photoflood lamps and were positioned behind the specimen with the aid of a photoelectric cell to obtain a fairly uniform light intensity at the reflective surface. Special care was required to insure that the lights did not impinge directly on the deflected model.

The camera employed throughout the study was a 4 x 5 Graphic View Camera, having a 135 Optar lens of f4.7 closed down to f 32. A desirable feature of this camera is that it permits focusing by movement of the ground glass plate. Initially, photographs were taken on Kodak Royal Panchromatic film through a 1/32 inch diameter pinhole located in a thin steel sheet attached behind the hole on the screen. Each exposure lasted 30 seconds. Later, it was found that more distinct photographs could be taken without the attached pinhole by use of Kodak Ortho type 3 film with each exposure lasting 60 seconds. However, when the attached pinhole was discarded it was necessary to use a 100 mm wide field Ektar lens when photographing the relatively large swept back wing model.

One of the significant problems concerned distortion of the photographs due to inaccurate positioning of the camera. Distortion can be minimized by locating the hole in the screen in line with the specimen surface and insuring that the film, screen and specimen surface are all parallel.

Control of the lighting in the room containing the test setup did not appear significant. However to obtain better definition of fringes in the vicinity of the model support structure, it was found necessary to darken these areas with black paint.

2.4   SUPPORT AND LOAD APPLICATION SYSTEMS

All of the tested specimens were clamped in the support fixture shown in Figure 2.5. Fittings were placed between the vertical I-beams and the specimen faces in order to provide a 2 in.width of support. All specimens were geometrically symmetric about the support centerline.

In loading, dead weights were applied simultaneously to corresponding points on either side of the centerline of support, thereby simulating the case of
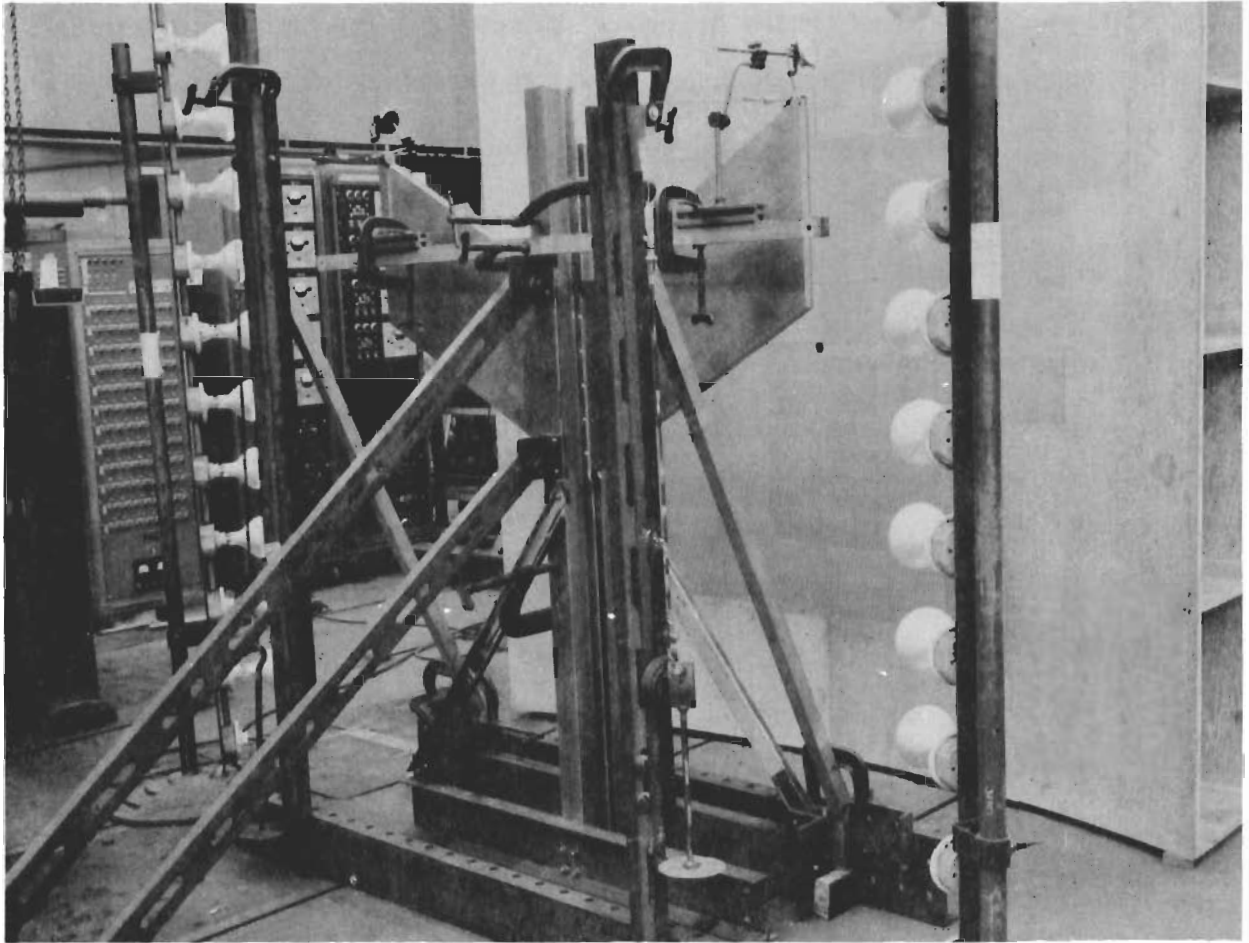
11

Figure 2.5 Test Setup, Rear View of Specimen

a cantilevered specimen. The loads were transmitted by wires to the underside of the specimen through a pulley arrangement.

Deflection measurements were made at the points of load application. These measurements were primarily to insure that the specimen deflections were symmetrical about the plate center line. Because of the relatively small support area and the application of loads by hand, control of this aspect of the test program was found to be quite important. In addition, these measurements were also to serve to verify the fringe technique data and the correspondence of the test results with published deflection solutions for the specimens. Dial gages, which could be read to the nearest 0.001 in., were employed for the deflection measurements (see Figure 2.6).
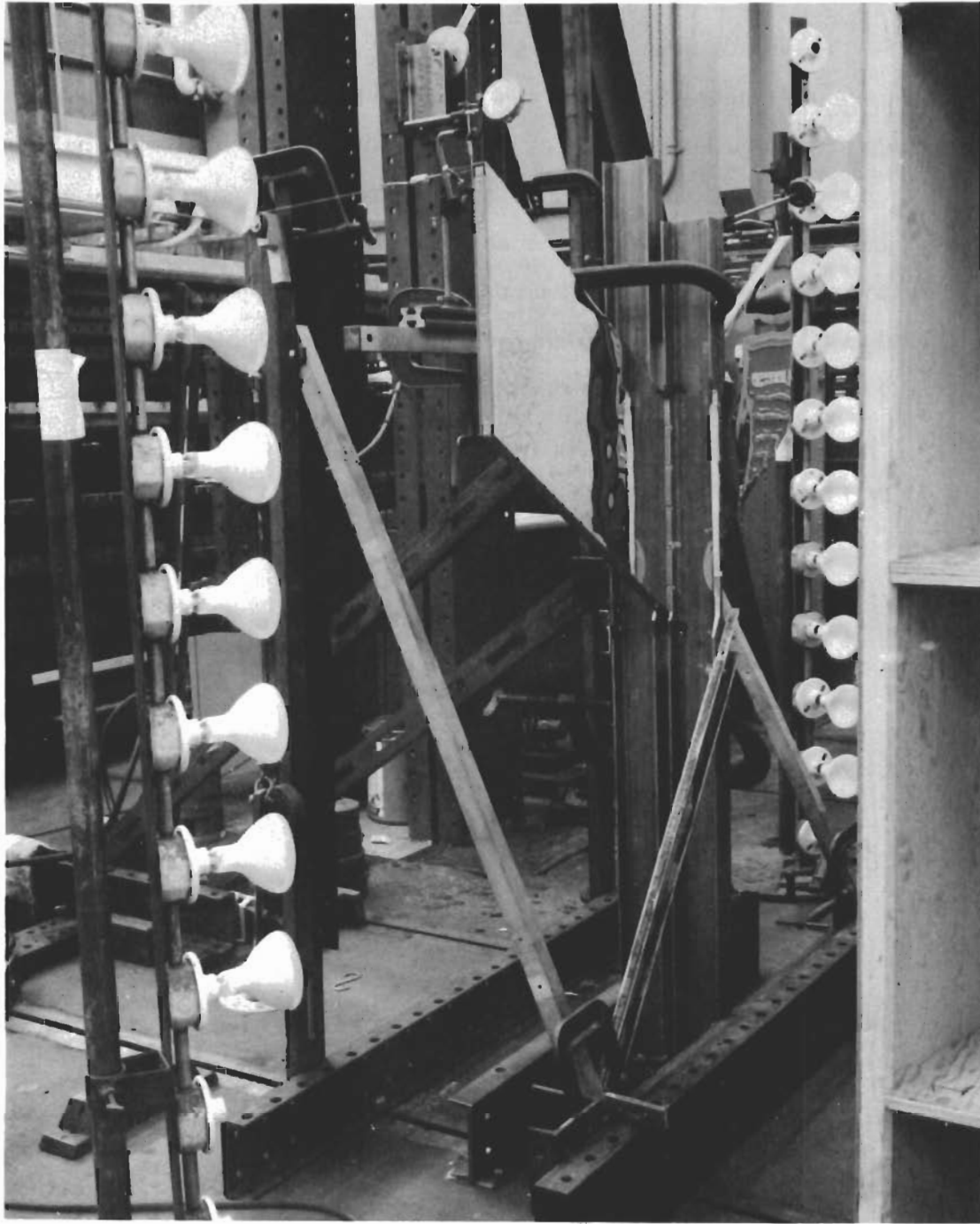
13

Figure 2.6 Test Setup, Front View of Specimen

14

SECTION 3.0

TEST SPECIMENS AND RESULTS

3.1 SQUARE PLATE

The square plate specimen is illustrated in Figure 3.1. This specimen was chosen to permit comparisons with known analytical solutions and with reliable test data obtained through the use of other test methods. It also served as a means for direct experimentation with different surface preparation techniques. These techniques are described below.

The specimen was 0.25 in. thick and composed of 7075-T6 aluminum alloy. The modulus of elasticity of this material can be taken as 10.4×10^6 psi; Poisson's ratio is 0.333. The total in-plane dimensions of the plate are 15 x 32 in., but due to clamping of the plate on a 2 in. support width, the total "exposed" semi-span measures 15 x 15 in.

Complete series of tests were conducted on this model for two types of surface preparation. In addition, numerous other surface preparation techniques were attempted with the specimen but were discarded when preliminary tests indicated they were lacking in merit.

Fringe patterns obtained for this plate are shown in Figures 3.2 through 3.5. Figures 3.2 and 3.3 pertain to the specimen with a polished surface. Figures 3.4 and 3.5 were obtained for the specimen with the vacuum metallized plastic sheet material attached to it. For each type of surface preparation, photographs were taken with both the large pitch of grid lines ($\frac{d}{2a}$ = 0.004 rad) and with the small pitch ($\frac{d}{2a}$ = 0.002 rad). The loading was restricted to a concentrated load at the tip corner point, magnitudes of 37.5 and 51.5 lb being employed for both the small and large pitches of grid lines. A 24.0 lb load level was utilized only with the small pitch.

15
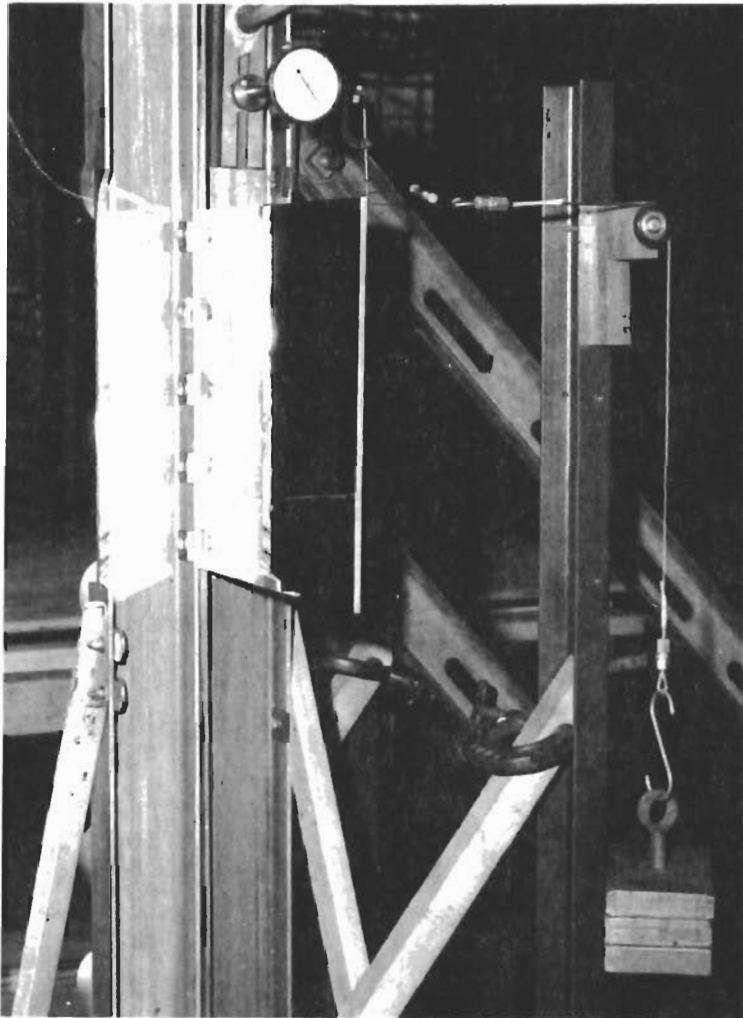
Figure 3.1 Square Plate Specimen

16
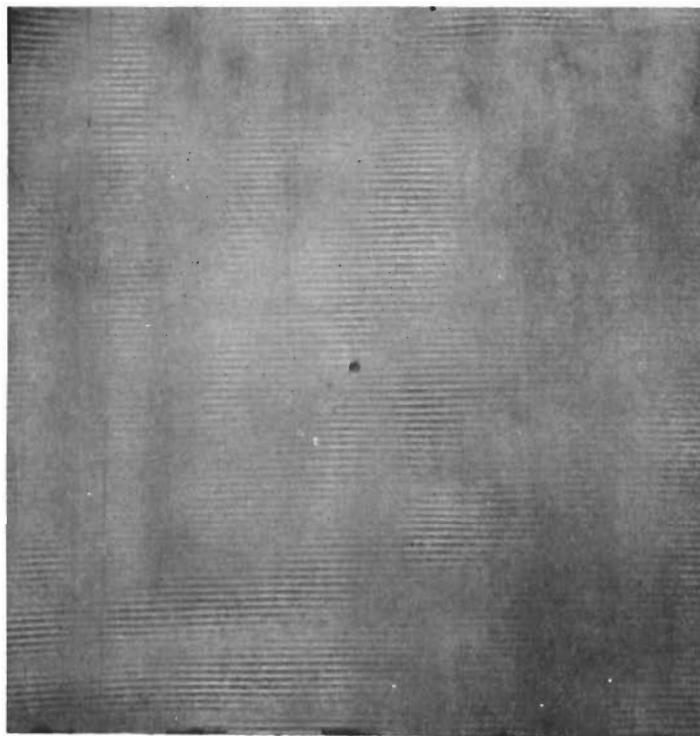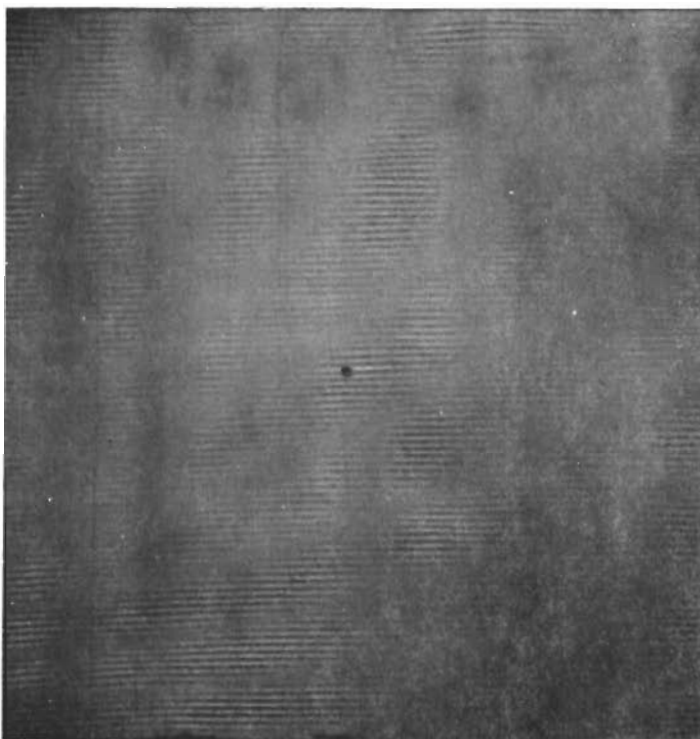
a. Load = 37.5 lb

b. Load = 51.5 lb

Figure 3.2. Fringe Photographs for Square Cantilevered Plate With

Polished Surface, Spanwise Slopes, $\Delta \dfrac{\partial w}{\partial x} = 0.004$ rad.
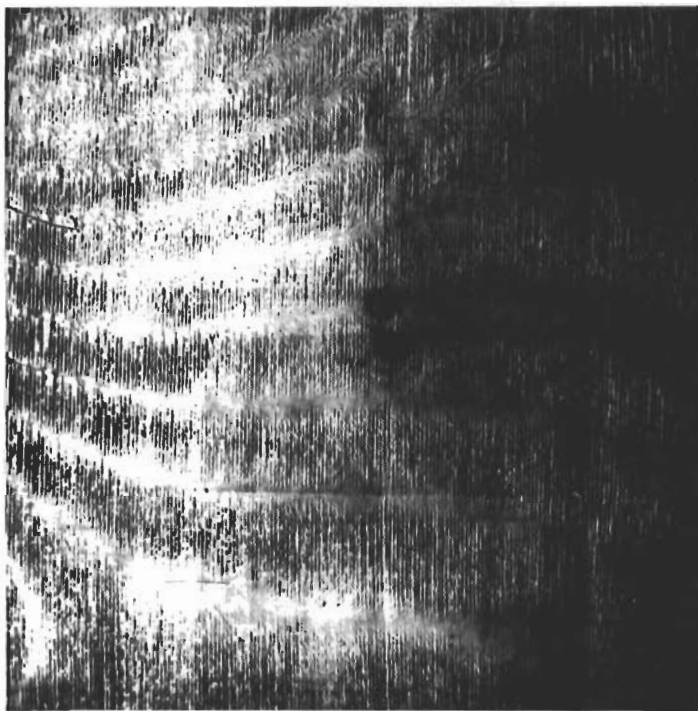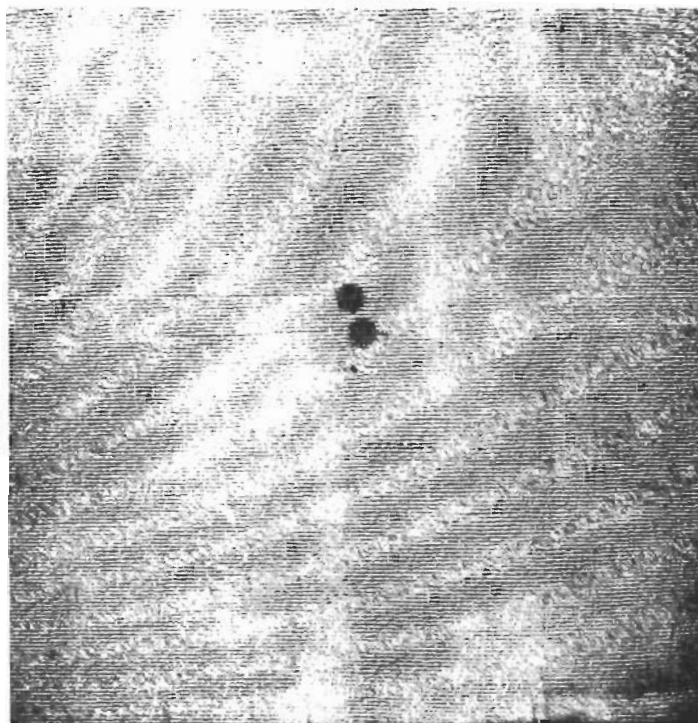
a. Load = 37.5 lb

b. Load = 51.5 lb

Figure 3.3. Fringe Photographs for Square Cantilever Plate With Mirrored 10 Mil Cellulose Acetate Film, Spanwise Slopes Due to 35.5 lb Load, $\Delta \dfrac{\partial w}{\partial x} = 0.002$ rad.

18
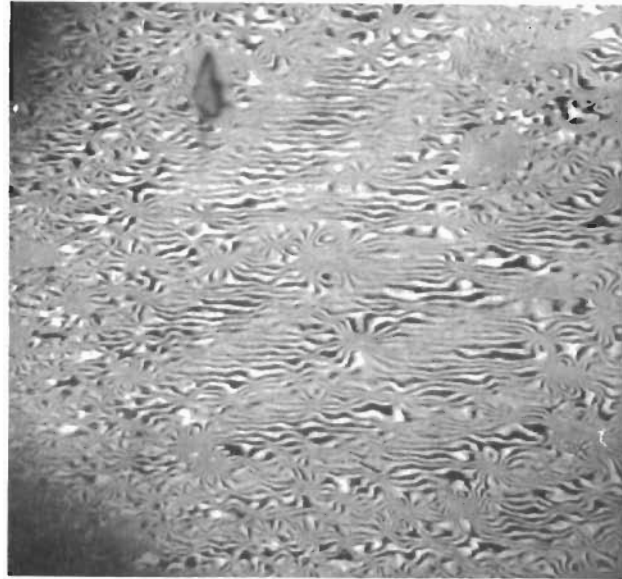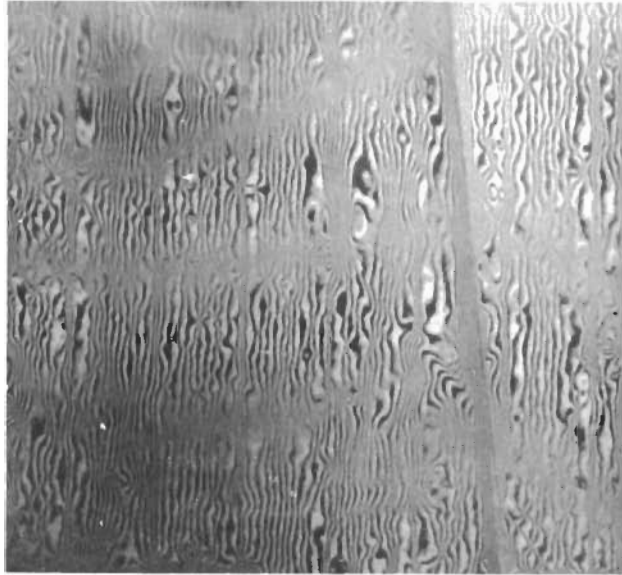
a. Chordwise Slopes, $\Delta \dfrac{\partial w}{\partial y} = 0.004$ rad. b. Chordwise Slopes, $\Delta \dfrac{\partial w}{\partial y} = 0.004$ rad. c. Spanwise Slopes, $\Delta \dfrac{\partial w}{\partial x} = 0.004$ rad.

(Adhesive Tape Attachment) (Adhesive Tape Attachment) (Attachment with Cement)

Figure 3.4. Fringe Photographs for Square Cantilevered Plate with
Mirrored 4 Mil Mylar Film

b. Attachment with Fluid
Glycerine and Water

a. Adhesive-Tape Attachment

Figure 3.5. Fringe Photographs for Square Cantilever Plate With
Mirrored 10 Mil Cellulose Acetate Film, Spanwise
Slopes Due to 35.5 Load, $\Delta \dfrac{\partial w}{\partial x} = 0.002$ rad.

20

Many of the tests were repeated in order to establish the reproducibility of the results. In every case it was found that the resulting fringe pattern photographs did not differ significantly from the results already obtained.
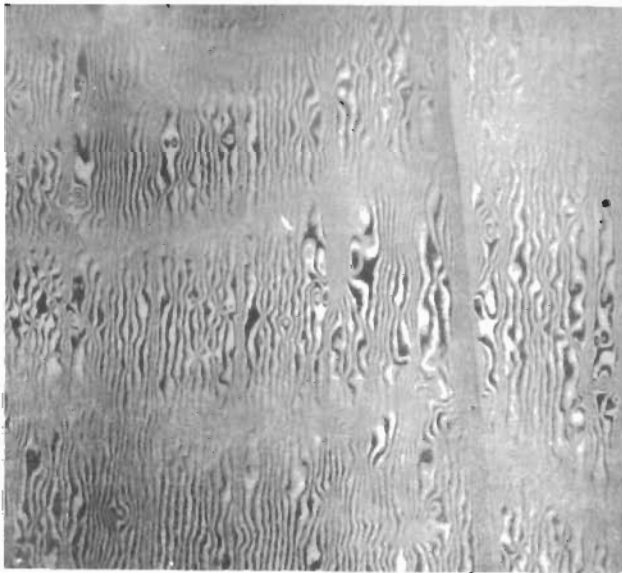
Techniques which can be employed to obtain a reflective surface can be grouped as follows:

(1) Direct polishing of the surface.

(2) Plating or coating of the surface with a reflective material.

(3) Attachment of a thin reflective sheet material to the surface.

The most direct method is using the surface in an as-received or polished condition. Previous investigations have largely been limited to this method, with various materials such as brass, aluminum, copper and steel being used for the specimens. It was found that a good surface can be obtained on copper by a special polishing treatment (Reference 1).

For any material, the reflectivity that can be obtained through polishing depends upon its metallurgical characteristics. It is desirable to have a material that is "specular"; i.e., a surface that is microscopically smooth so that the largest proportion of the light intensity is preserved when reflected. Pure aluminum is excellent in this regard. It is reported in Reference 2, however, that polishing the materials cited above resulted in the distortion of the grid line reflections. Nevertheless, quantitative experimental data was obtained. Other common metals of which structures are often composed (e.g., steel) appear to be unsatisfactory from the standpoint of polishing.

In consequence of the difficulties related to attaining a good reflective surface for metallic plates by polishing, most reported experiments with polished surfaces have been performed on relatively small plate models of plastic material. Black opaque acrylic plastic sheet material, with good reflective qualities already included, has been most commonly employed.

In attempting to polish the plate specimen, conventional rotary polishing equipment was first employed. Preliminary tests were then conducted with the

specimen. Fringe patterns obtained with this surface using the 0.16 in. grid line width were fairly distinct. However, use of the 0.08 in. width resulted in barely distinguishable fringes. Better and usable results were obtained after extensive hand polishing of the plate. Such polishing was directed at eliminating surface oxides at locations as indicated on repeatedly taken photographs. In general, it appears that the value of $\frac{d}{2R}$ for which the equipment is designed depends on the degree of surface optical flatness or reflectively that can be attained. However, the attainment of optically flat surfaces on practical structures, although feasible in many cases, would prove prohibitively expensive.

In investigations of the second approach to surface preparation, it became evident that a new electroplating brush process (the "Dalic" process)* would be most promising. This process permits a desirable coating, such as pure aluminum, to be deposited to a desired thickness. Small sample surfaces prepared by this process, however, revealed that it is expensive and requires additional development for application to relatively large surfaces.

Examination of choices posed by the third approach (attachment of a thin reflective sheet material to the surface) led to the most satisfactory of all the schemes for providing a reflective surface. In this scheme, as suggested in Reference 1, plastic sheets are silvered and attached to the specimen. To minimize effects on stiffness it is desirable that relatively thin sheets be used. From a survey for suitable materials it was found that the surfaces of thin sheet material of cellulose acetate, mylar and plexiglass can be given an excellent mirrored surface by the vacuum metallizing process.

Plastic sheets ranging in thickness from 1 to 10 mils were vacuum metallized. Initially, these mirrored surfaces were relatively flat (when compared with a conventional glass mirror) except for the smaller sheet thickness, 1 and 2 mils,

---

* The Dalic process is a brush electroplating technique developed by Sifco Metachemical Inc., Cleveland, Ohio.

which were slightly wavy. However, attachment of the mirrored sheets to the model surface by various means resulted in wavy surfaces which created severe reflective distortions and a number of such attachment schemes had to be examined and attempted experimentally.

Among the attachment techniques studied were:

(1) The use of stickyback tape (adhesive backed tape)

(2) Fluids of differing viscosity and

(3) Cements or adhesives.

In general, the thinner sheets could be readily attached to the surface by any one of the methods, but not to the flatness desired. Typical results are shown in Figures 3.4 and 3.5.

The use of stickyback tape results in a surface with waves which depend critically on the care with which the mirrored surface is applied. This is because the plastic sheet is applied by pressing it on the surface with a pressure which could not be adequately controlled. Typical fringes obtained with this attachment technique are shown in Figure 3.4a and b for a 4 mil mylar film and in Figure 3.5a for a 10 mil cellulose film. Despite the distortion shown in these figures, the general adequacy of the fringe patterns obtained were comparable, quantitatively, to those obtained from the polished flat plate. However, for those situations in which the fringes are closely spaced (as a consequence of larger loads or smaller grid line widths) the distortions introduced create untenable fringe discontinuities. It was found that these distortions tend to decrease with mirrored sheet thickness, but for the thicknesses at which such improvements become significant the attachment bond fails. The bond failure is due to the larger stiffness of the thicker mirrored sheets which require a stronger adhesive to hold them to the specimen when deflected.

Use of various fluids with different viscosities resulted in fairly smooth surfaces for the less viscous fluids such as water. These surfaces, however, tended to slip and peel with time. More viscous fluids such as glycerine possessed the required bonding strength needed to avoid the above difficulties, but voids and
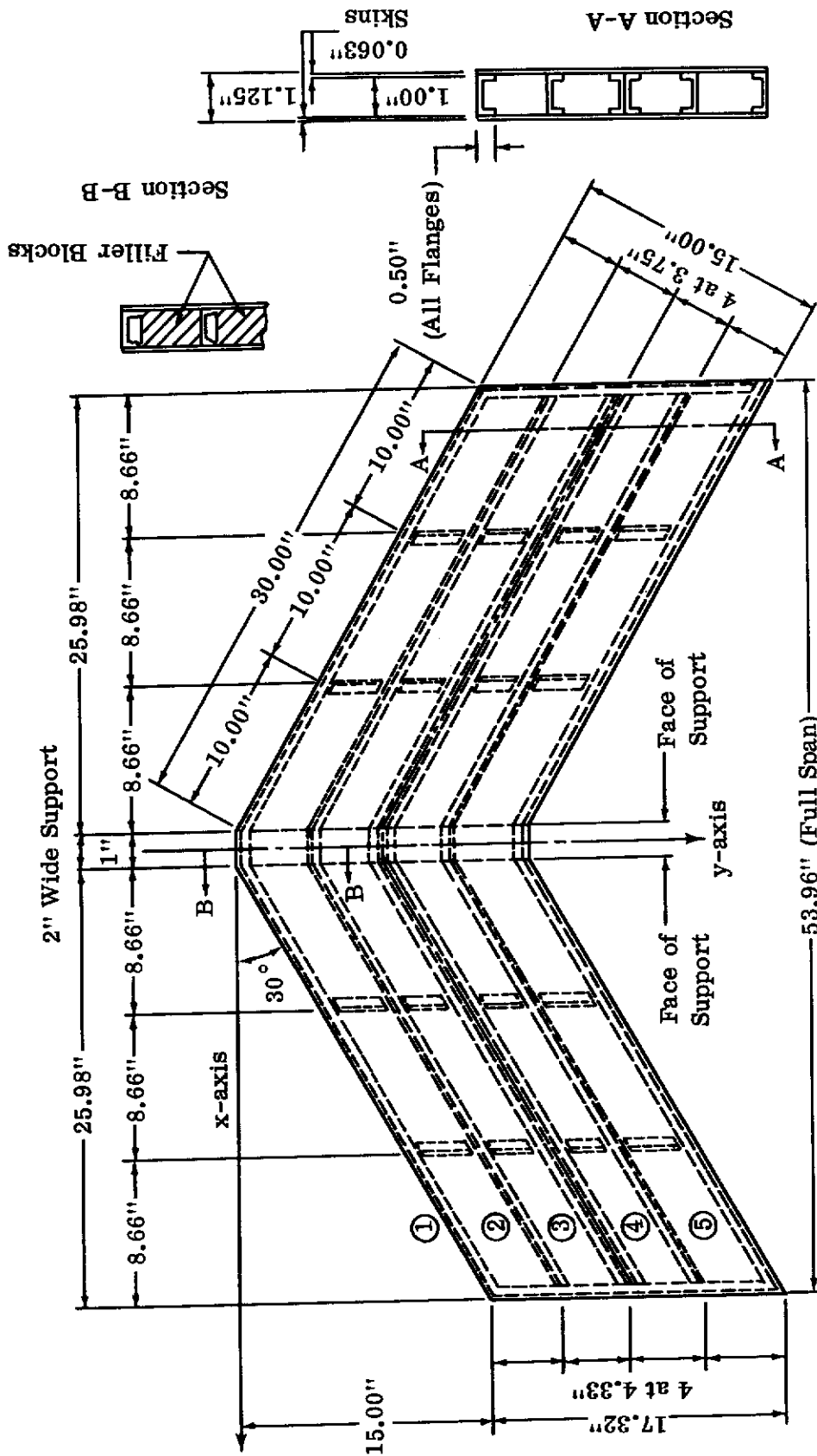
globules of this liquid found in the plate to plastic sheet interface could not be eliminated. This condition resulted in a wavy surface. Fringes taken with this attachment technique are shown in Figure 3.5b.

Bonding of the mirrored plastic sheets to the specimen surface with a bonding cement eliminated the peeling problem attendant with the other two attachment techniques. Nevertheless, other difficulties present themselves. Uniform application of the bonding cement was not possible and the consequent variation in bond thickness introduced pronounced waviness in the reflective surface. In addition, it was found that as a result of not being able to satisfactorily control the bonding of such large surfaces, relatively large voids or spaces in the bond were present which tended to close or open during the application and removal of the loads. Such behavior introduced additional distortions in the fringe patterns obtained. One important shortcoming of this method is that once applied, the plastic sheet is often difficult to remove. A typical photograph obtained with this attachment technique is shown in Figure 3.4c..

3.2 SWEPT WING MODEL

The swept wing model is illustrated in Figure 3.6. This model was fabricated and tested for displacement influence coefficients at the spar-rib intersection points in conjunction with an evaluative study of wing analysis methods (see References 5 and 6). It is composed of 6061-T6 aluminum alloy ($E = 10.6 \times 10^6$). The skins are single sheets of 0.063 in. thick, flush-riveted to 0.040 in. thick formed channel internal members. The spar channels are continuous from tip to tip, the rib segments being joined to these by means of clip angles.

In the design of this model it was intended that during test it be clamped in a 2-in. wide support along the y-y axis and loaded symmetrically about this axis. To preclude severe clamping effects a set of solid internal members (i.e., "blocks") were provided in the support area. Tests described in Reference 5 were limited to the application of loads to the spar-rib intersection points in such a manner and sequence that a complete set of displacement influence coefficients were obtained for all such points.

24

Section A-A

Skins

0.063"

1.125"

1.00"

Section B-B

Filler Blocks

0.50"
(All Flanges)

15.00"

4 at 3.75"

10.00"

A

10.00"

A

30.00"

10.00"

Face of
Support

8.66"

y-axis

8.66"

Face of
Support

25.98"

53.96" (Full Span)

2" Wide Support

1"

8.66"

B

B

30°

x-axis

8.66"

25.98"

8.66"

① ② ③ ④ ⑤

8.66"

4 at 4.33"

17.32"

15.00"

PLANFORM

NOTES: Model material – 6061–T6 Aluminum.

All internal members formed of
0.040" sheet.

Figure 3.6 Geometry and Structural Details of Swept Wing Model

Both of the techniques for surface preparation which had proved success-ful for the rectangular plate specimen (polishing and the attachment of reflective sheets) were attempted with this model. First, the surface of this model was polished with a large rotating disc, using fine polishing compounds; isolated portions of the surface were hand polished where it appeared to be necessary.

Fringe patterns obtained from tests of the polished model did not prove to be interpretable. This was due, primarily, to the presence of flush head rivets and accompanying indentations on the surface. Fringes in the vicinity of the rivets were discontinuous and ill-defined. In addition, other surface imperfections in the form of scratches and local waviness incurred during fabrication or previous testing were detrimental. Reflective surface conditions probably could have been improved by further polishing with improved techniques but this would entail the removal of a significant portion of the model surface and thereby lead to inaccurate results.

The use of vacuum metallized plastic sheets to provide a reflective sur-face led to the only interpretable fringe patterns. Series of tests with two such arrangements were conducted. In the first series the sheets were 0.006 in. thick cellulose acetate, attached to the surface with stickyback tape. Fringe photographs taken with use of this scheme are shown in Figure 3.7 and 3.8. Only the small pitch of grid lines ($\frac{d}{2a} = 0.002$) was employed for these tests.

In the second series, the sheet material was plexiglas, 0.04 in. thick. These sheets were attached to the surface by means of an epoxy adhesive. Loadings were applied only as required to indicate if interpretable fringes could be obtained. The limited results indicated that results of a more formal testing sequence would be much the same as those obtained with the cellulose acetate-stickyback tape scheme.
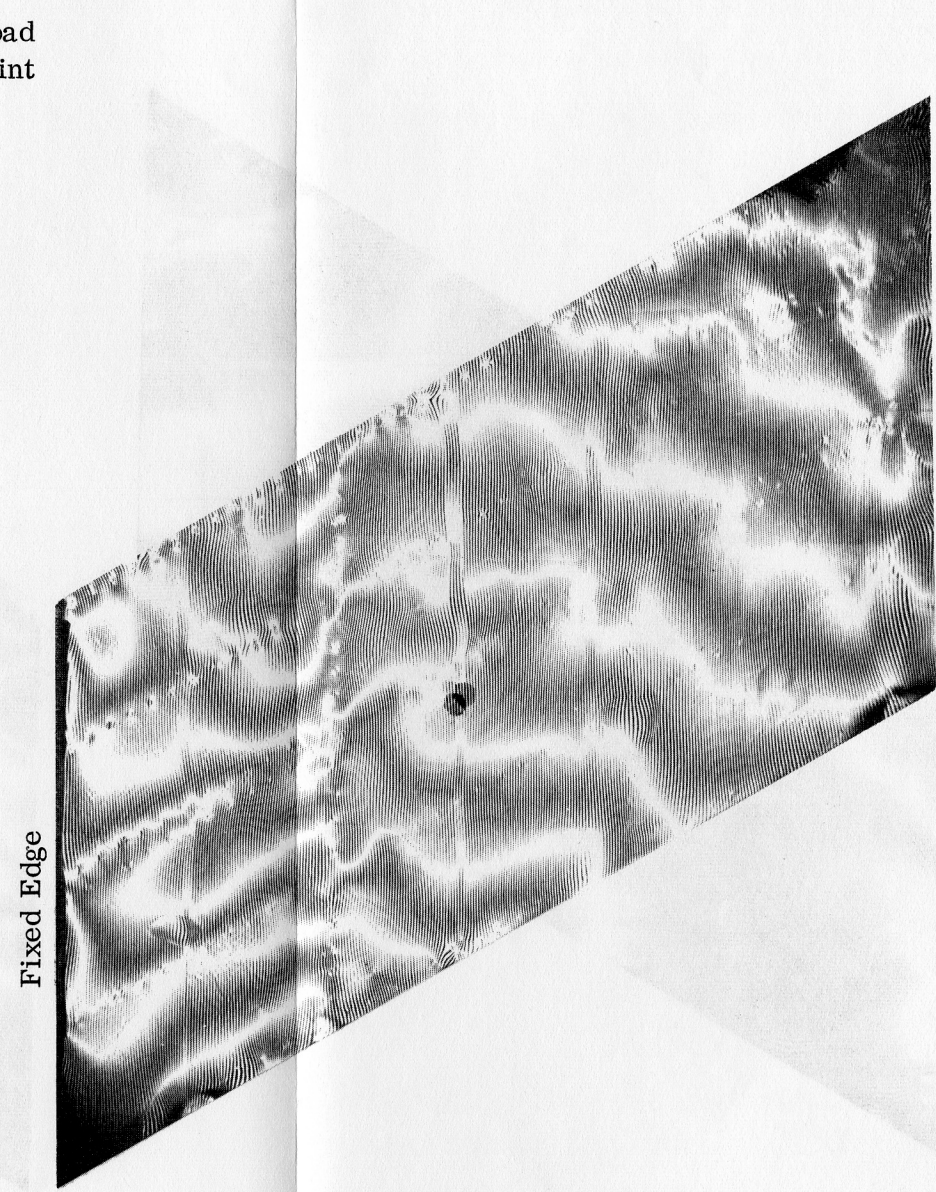
Load
Point

Load
Point

Fixed Edge

Fixed Edge
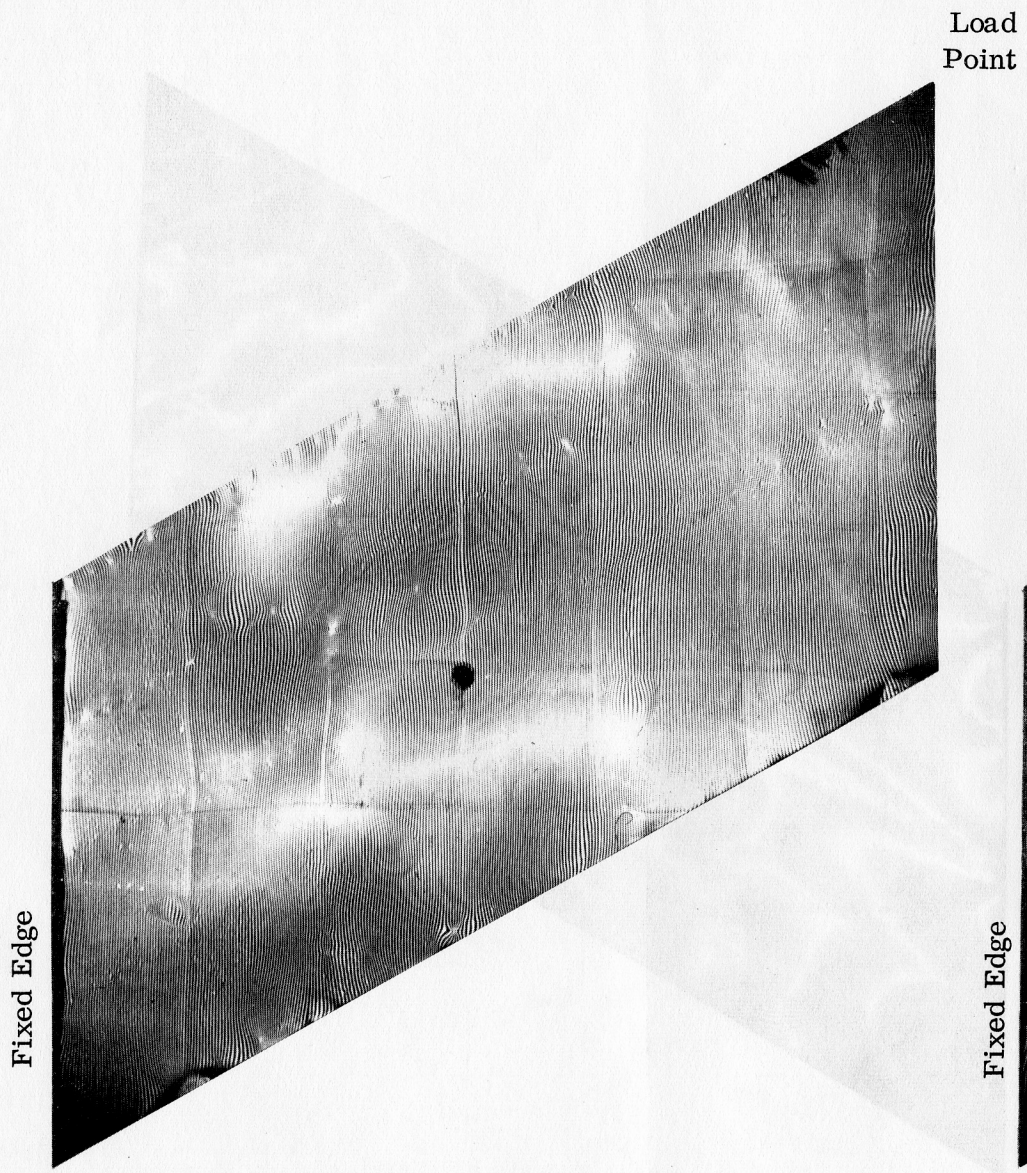
Fixed Edge
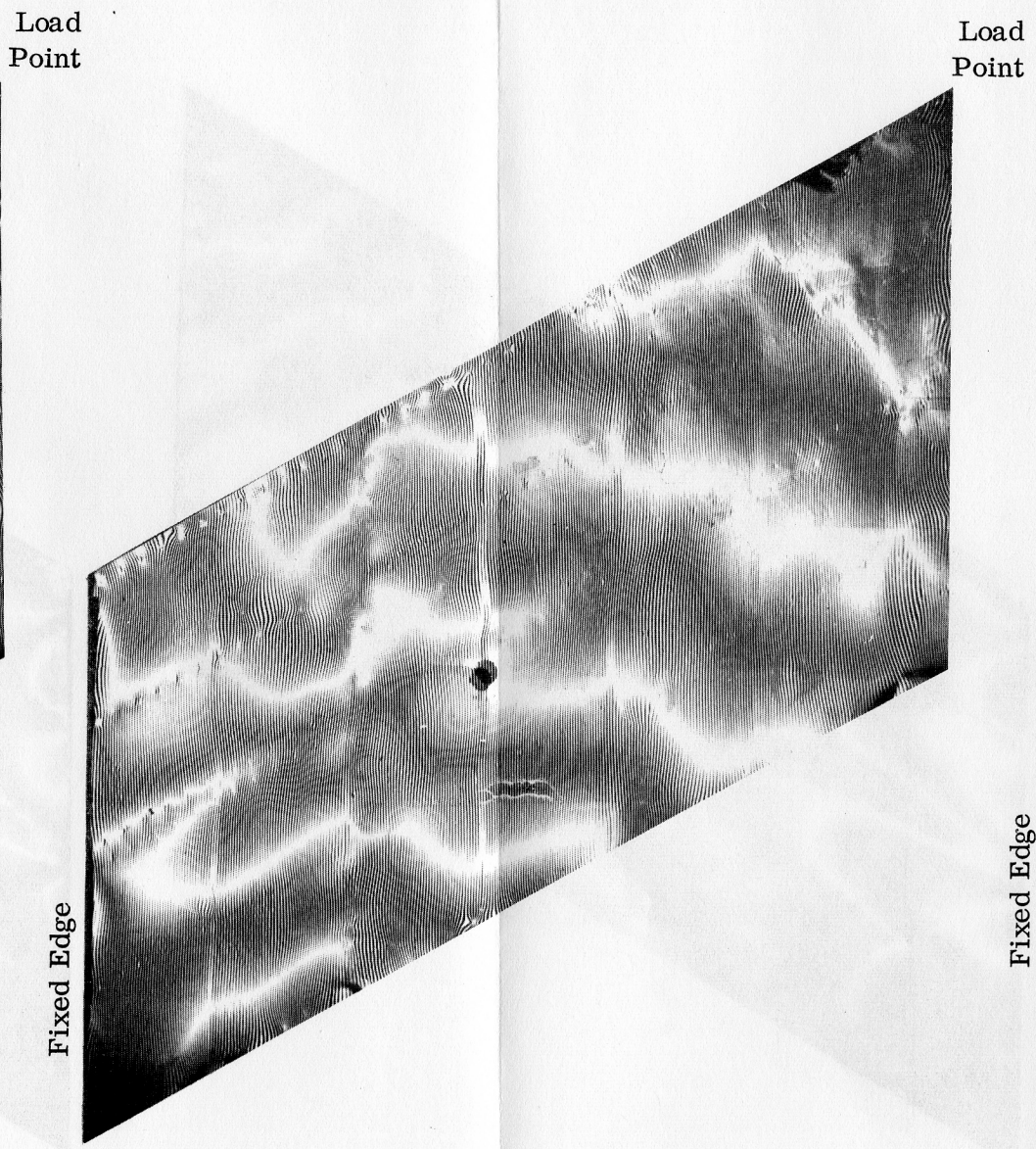
a. Load = 44.3 lb

b. Load = 89.9 lb

c. Load = 136.9 lb

Figure 3.7 Swept Wing Model – Fringe Photographs for Chordwise Slope Changes ($\Delta \frac{\partial w}{\partial x}$)
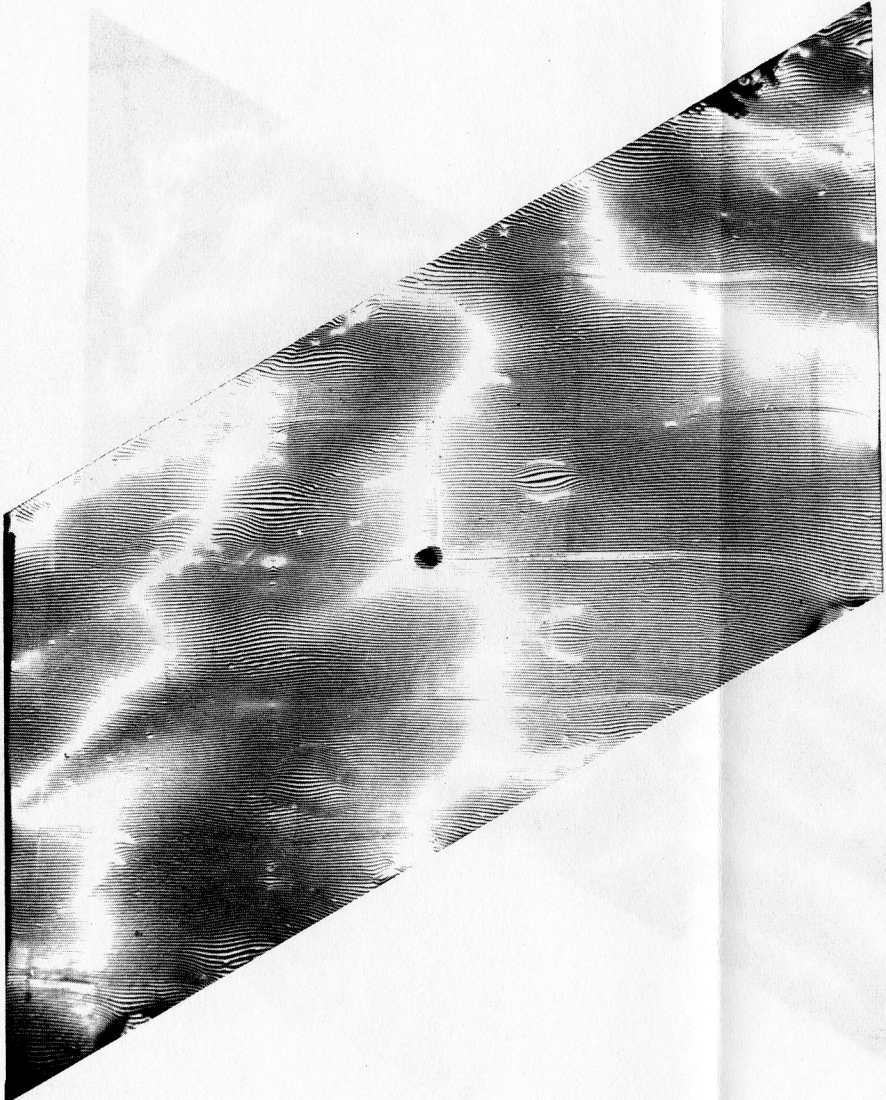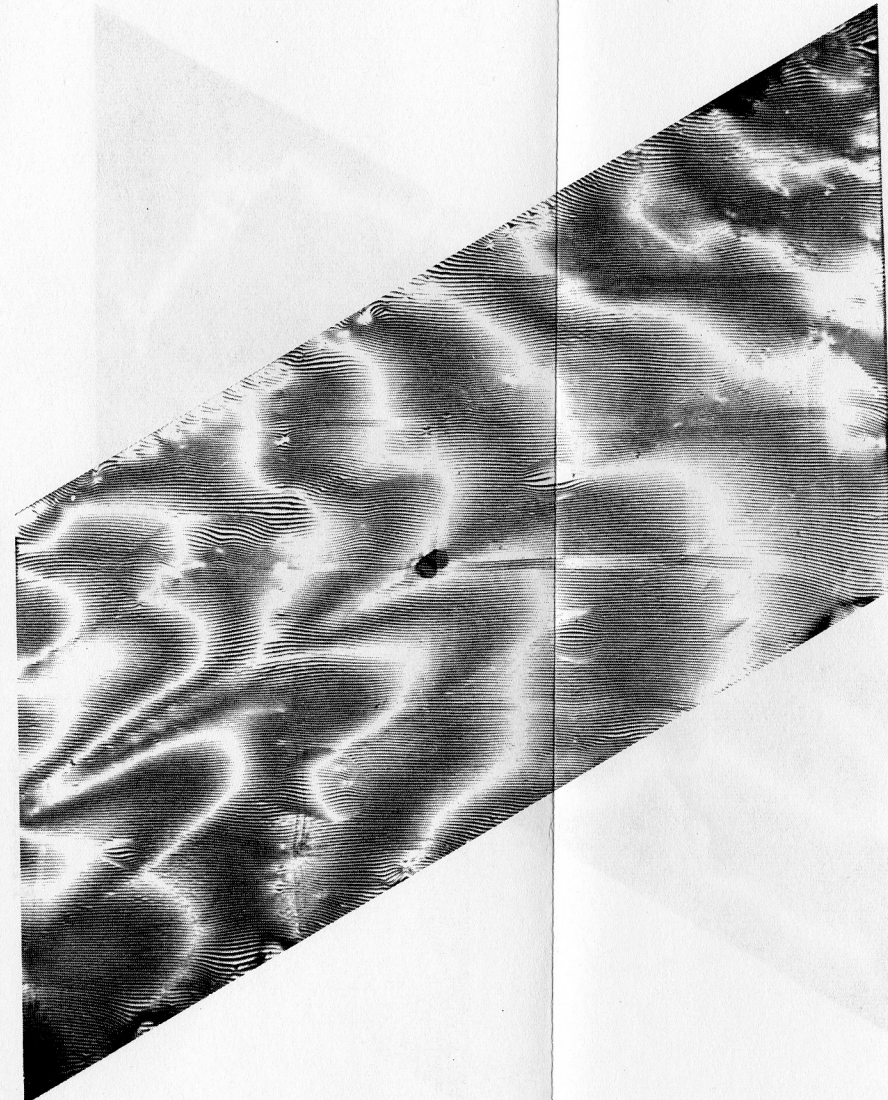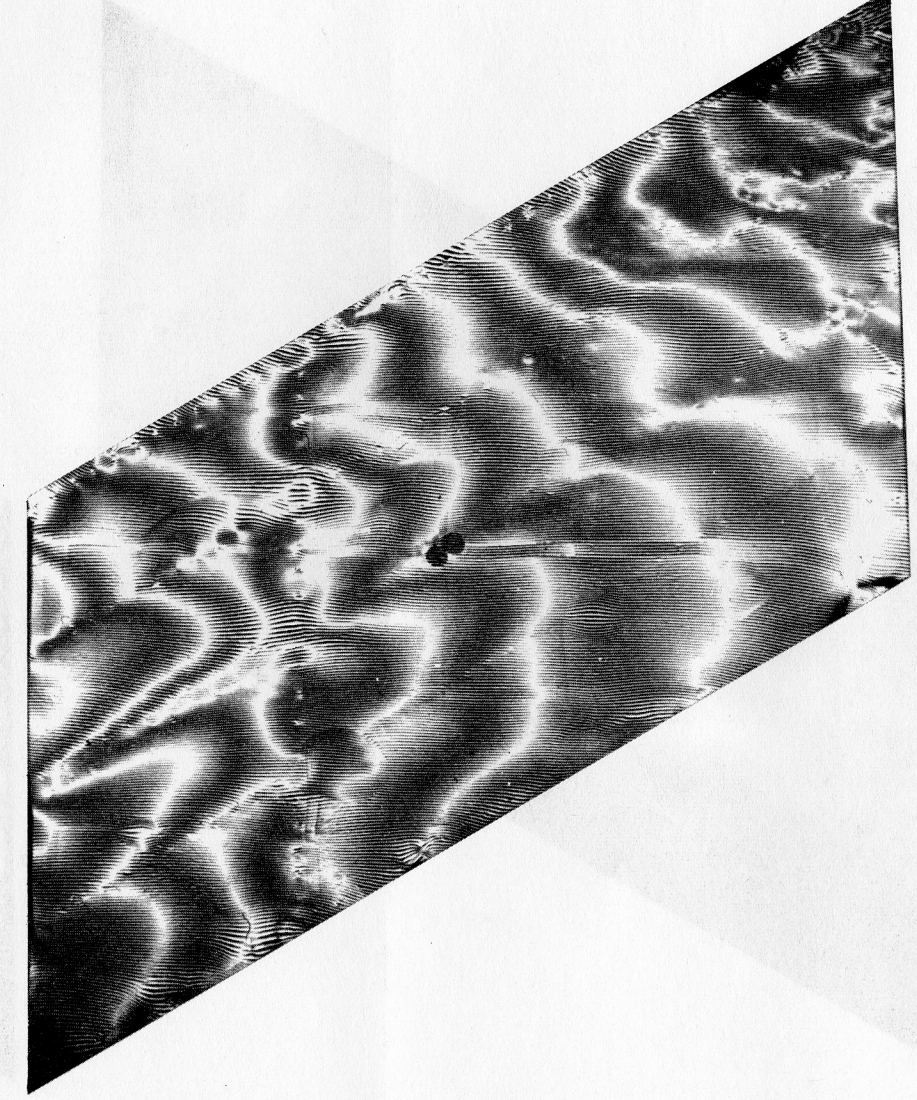
27

Fixed Edge

a. Load = 44.3 lb

b. Load = 89.9 lb

c. Load = 136.9 lb

Figure 3.8 Swept Wing Model – Fringe Photographs for Chordwise Slope Changes ($\Delta \dfrac{\partial w}{\partial y}$)

28

SECTION 4.0

## ASSESSMENT OF RESULTS

4.1 SQUARE PLATE

Figures 3.2 through 3.5 disclose that the slope contours (fringes) obtained from the plate with the attached vacuum metallized plastic sheet did not differ significantly from those obtained from the bare polished surface. Thus, the local distortions in the photographs due to the presence of small waves in the sheet were not important except for the larger loads where the fringes are more closely spaced.

It is also noteworthy that the application of the plastic sheet to the surface in separate pieces did not significantly impair the continuity of the fringes. This leads to the conclusion that large test surfaces can be covered with more easily obtained small sheet segments without adversely affecting the measured results.

In order to achieve comparisons with test data published elsewhere and with analytical solutions, the photographed fringe patterns were reproduced as line drawings as shown in Figures 4.1 and 4.2. In most cases the slope contour lines were recorded by tracing directly from modestly enlarged photographs. In some cases, however, the fringe definition was so vague as to require an extremely large (4X) enlargement of the photograph and only the light fringes could be delineated by noting the breaks in the dark lines.

To provide a further and more unified basis of comparison, all results were nondimensionalized with respect to the parameters $\dfrac{D}{aP}\dfrac{\partial w}{\partial x}$ and $\dfrac{D}{aP}\dfrac{\partial w}{\partial y}$, where D is the plate flexural rigidity $\left(\dfrac{Eh^3}{12(1-\mu^2)}\right)$ and P is the value of the applied load at the tip corner point. To effect this nondimensionalization, the following values were employed: $E = 10.4 \times 10^6$ psi, $h = 0.25$ in. and $\mu = 0.333$. These nondimensionalized experimental results, representing the spanwise and chordwise slope contours for a tip corner point concentrated load condition, are plotted in Figures 4.3 and 4.4. It should be noted that the separate plotting of results from the

29
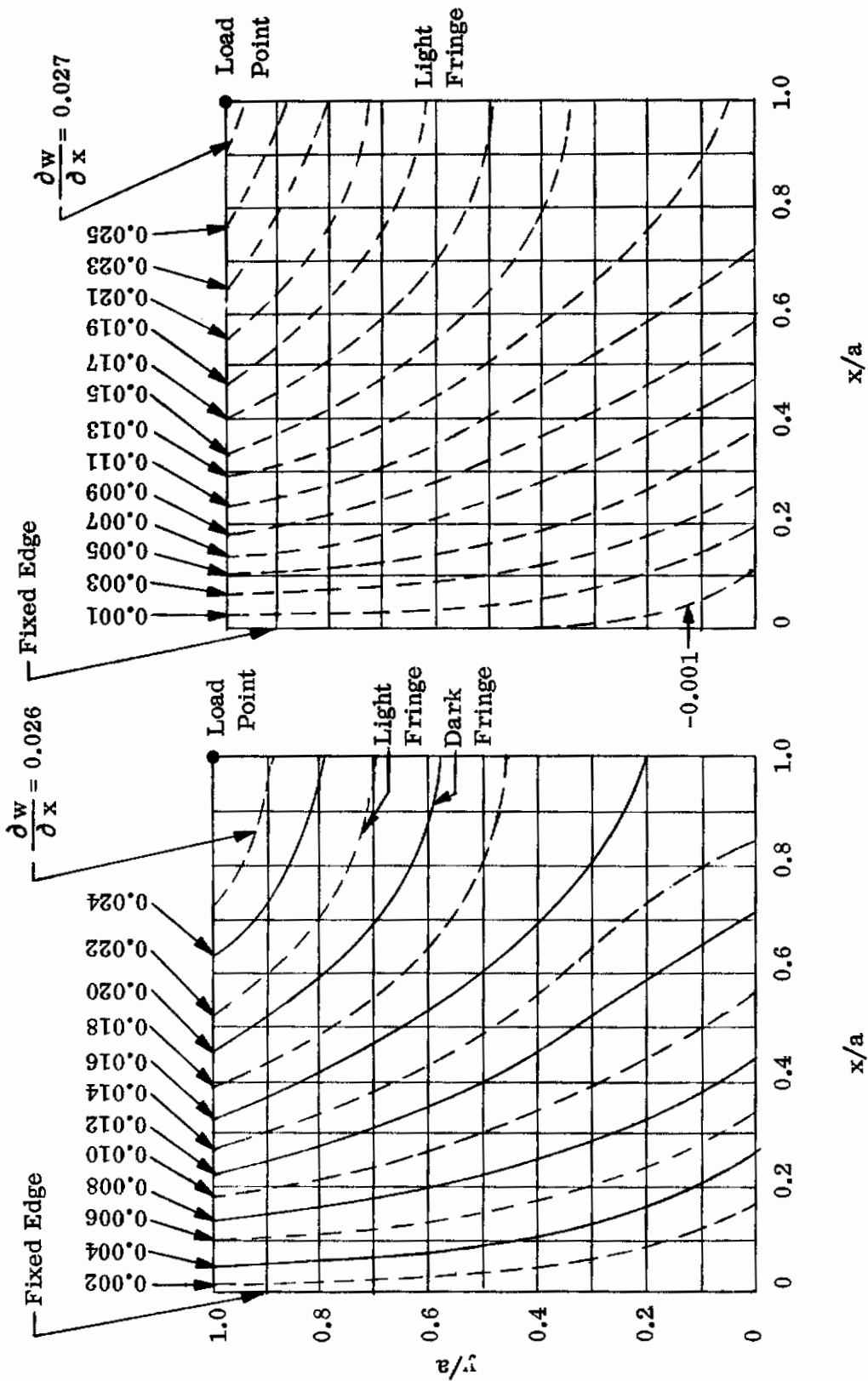
a. Results for $\Delta \dfrac{\partial w}{\partial x} = 0.004$ rad

b. Results for $\Delta \dfrac{\partial w}{\partial x} = 0.002$ rad

Figure 4.1. Square Cantilevered Plate – Contour Lines for $\dfrac{\partial w}{\partial x}$ (Load = 37.5 lb)

Figure 4.2. Square Cantilevered Plate – Contour Lines for $\dfrac{\partial w}{\partial y}$ (Load = 51.5 lb)
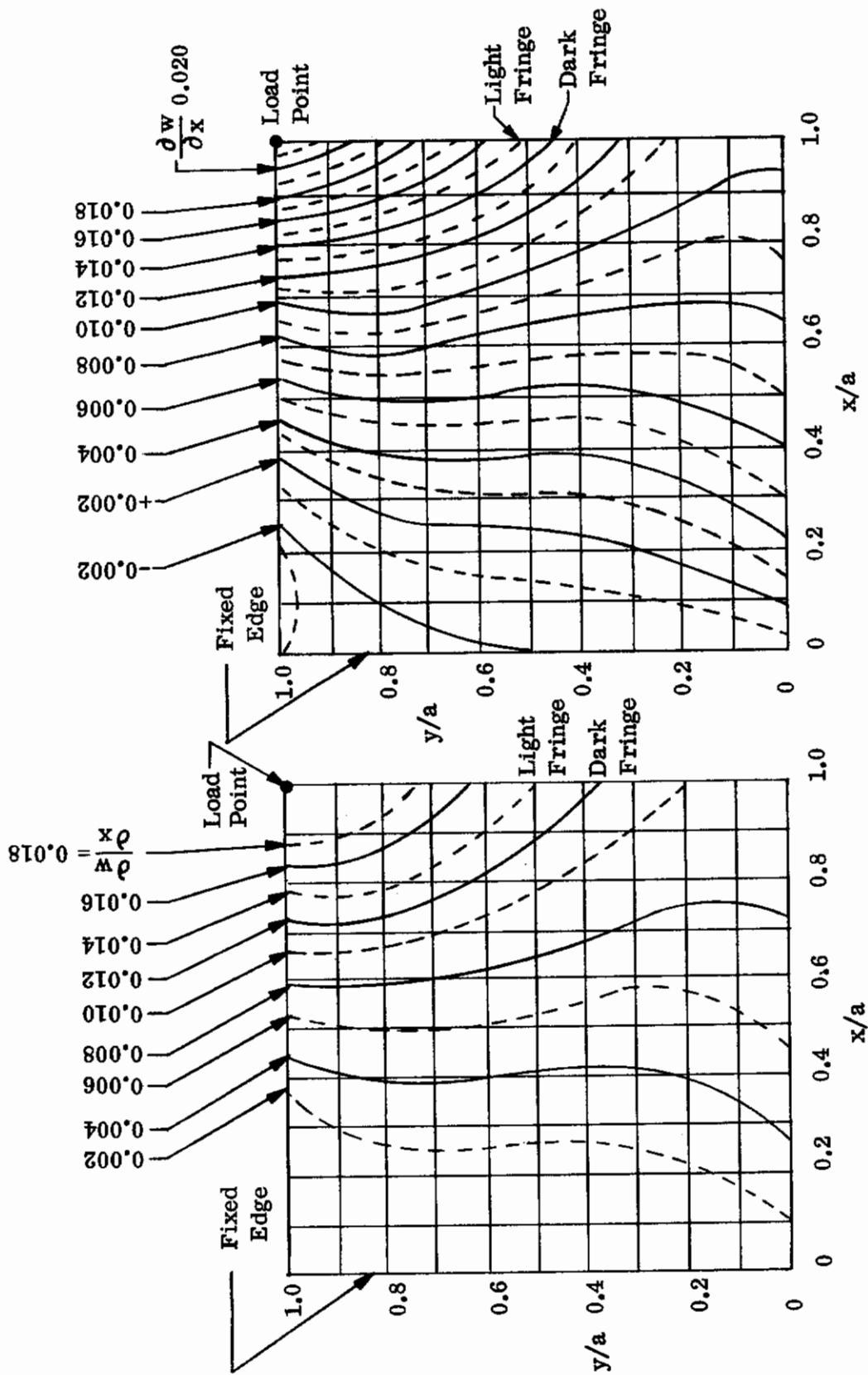
a. Results for $\Delta \dfrac{\partial w}{\partial y} = 0.004$ rad

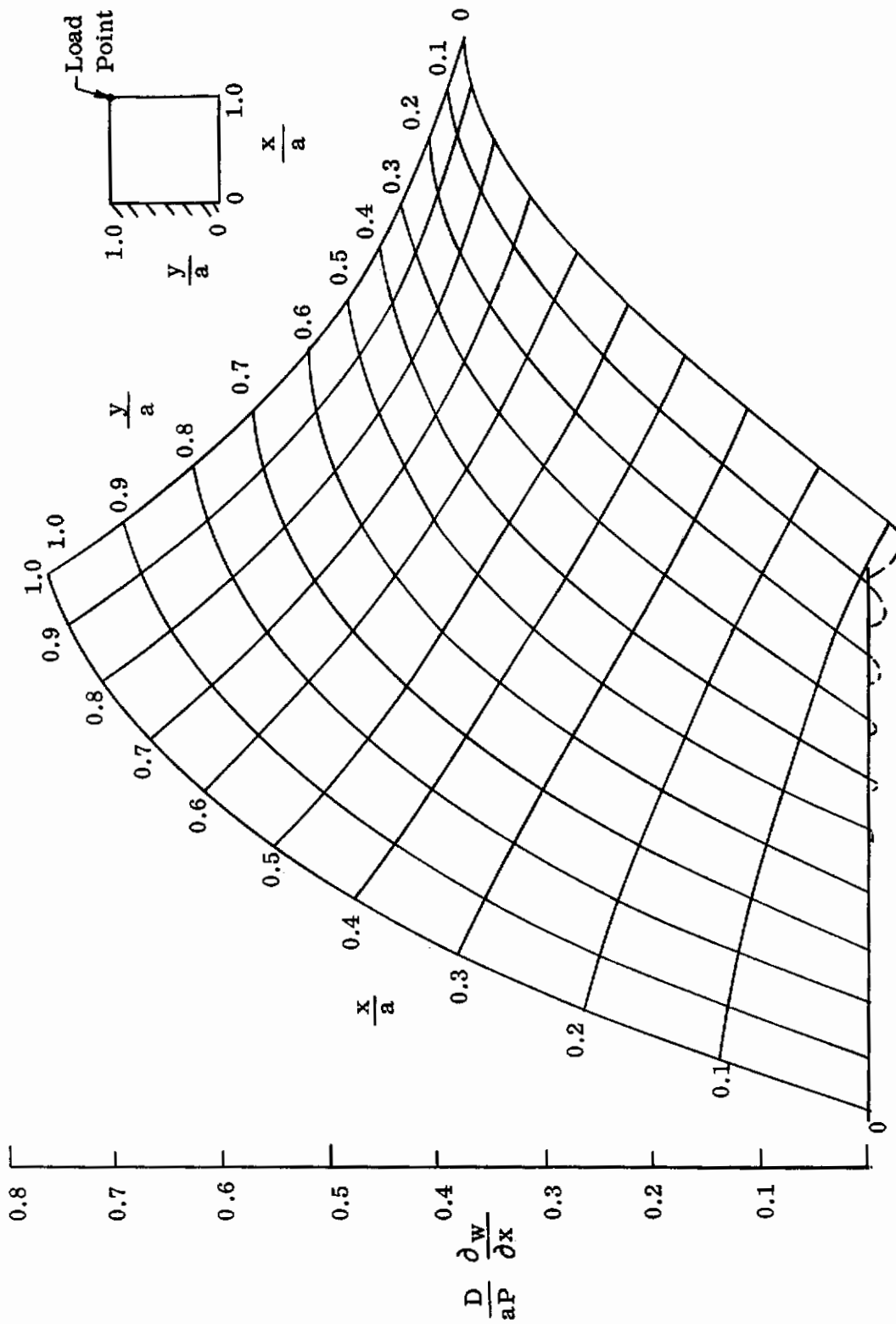b. Results for $\Delta \dfrac{\partial w}{\partial y} = 0.002$ rad

31

Figure 4.3. Square Cantilevered Plate – Experimental Spanwise Slope Influence Coefficients ($\Delta \dfrac{\partial w}{\partial x} = 0.002$ rad)
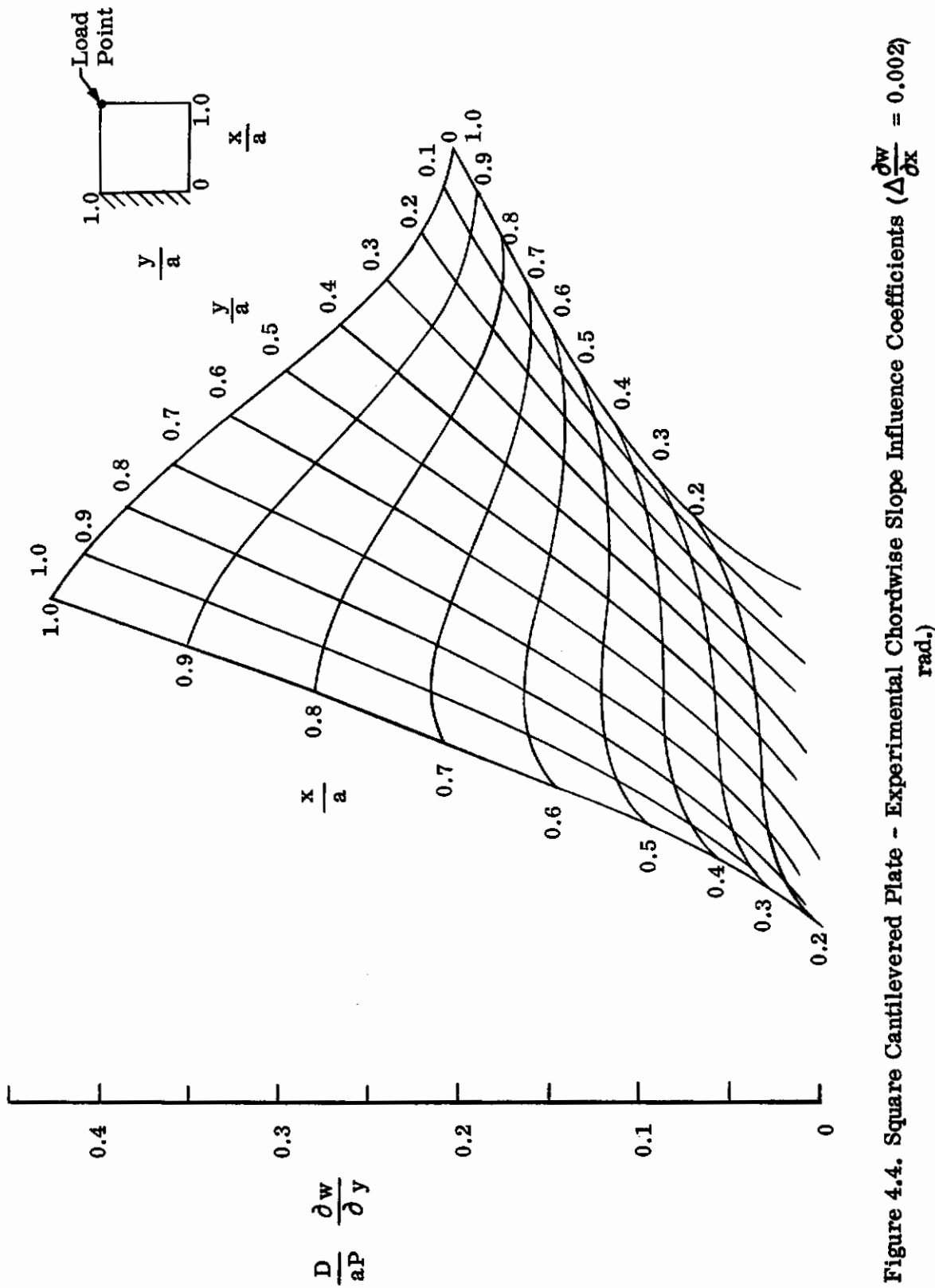
Figure 4.4. Square Cantilevered Plate – Experimental Chordwise Slope Influence Coefficients ($\Delta\frac{\partial w}{\partial x}$ = 0.002 rad.)

33

small and large grid line width experiments, respectively, leads to essentially the same results. The results plotted are those for the smaller grid line width ($\frac{d}{2a} = 0.002$).

The analytical results employed in comparisons of the Moire' fringe data were obtained with use of a matrix displacement technique. This technique, described in Reference 7 , utilizes rectangular discrete elements for idealization of the actual structure. Relationships for the discrete elements are based on an assumed deflectional pattern within the element and use the differential equations of plate flexure in their development. The grid work for the analysis of the subject specimen appears in Figure 4.5. Results are obtained directly in terms of slope displacements at the grid points. These slopes (or slope influence coefficients) for the chordwise and spanwise directions, respectively, are presented in carpet plot form in Figures 4.5 and 4.6. It should be noted that these results are based on consideration of plate flexure alone and do not include the effects of shear displacements.

Comparison of Figures 4.3 and 4.4 with 4.5 and 4.6 shows a generally close agreement between theory and test. In fact, the theory and test results are not superimposed on a single plot due to the complexity that would be occasioned by their closeness. Instead, the more explicit comparisons provided by representation of contour lines for slope influence coefficients are given (Figures 4.7 and 4.8). It is seen from these that the theory and test results compare to approximately the same extent for both $\Delta \frac{\partial w}{\partial x} = 0.004$ and $\Delta \frac{\partial w}{\partial x} = 0.002$. All results appear to become less accurate as the tip chord is approached, the spanwise slopes $\left(\frac{\partial w}{\partial x} \right)$ being less affected in this regard than the chordwise slopes $\left(\frac{\partial w}{\partial y} \right)$.

It can be concluded from these results that the subject experimental technique provided a relatively high degree of accuracy in view of the many factors which may have adversely affected accuracy. The latter include support flexibility, inaccuracies in load measurement, and the neglect of shear displacements and inaccuracies in material property data in the formulation of the comparative analyses.
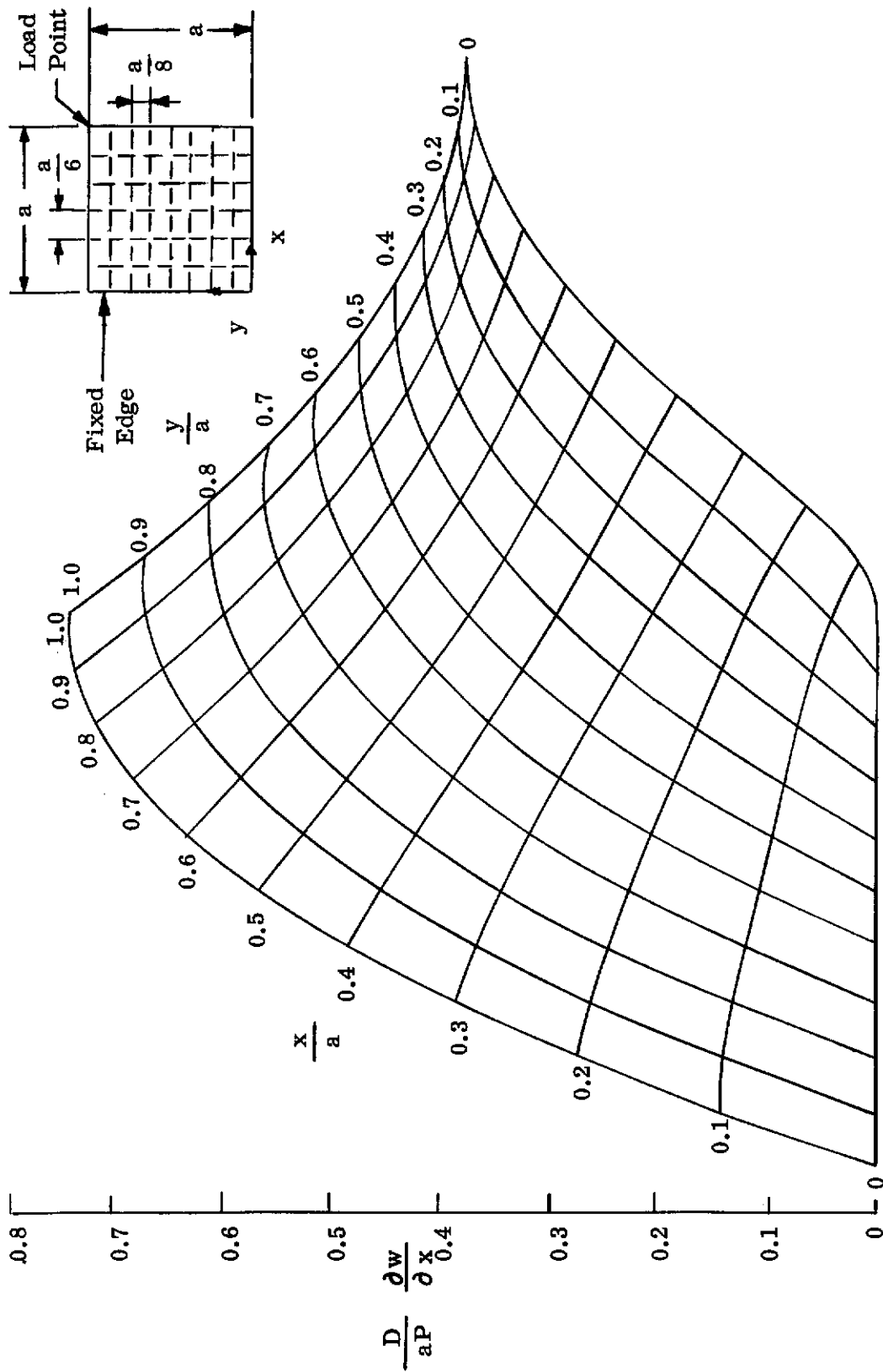
34

Figure 4.5. Square Cantilevered Plate Analytically Derived Spanwise Slope Influence Coefficients for Corner Point Load
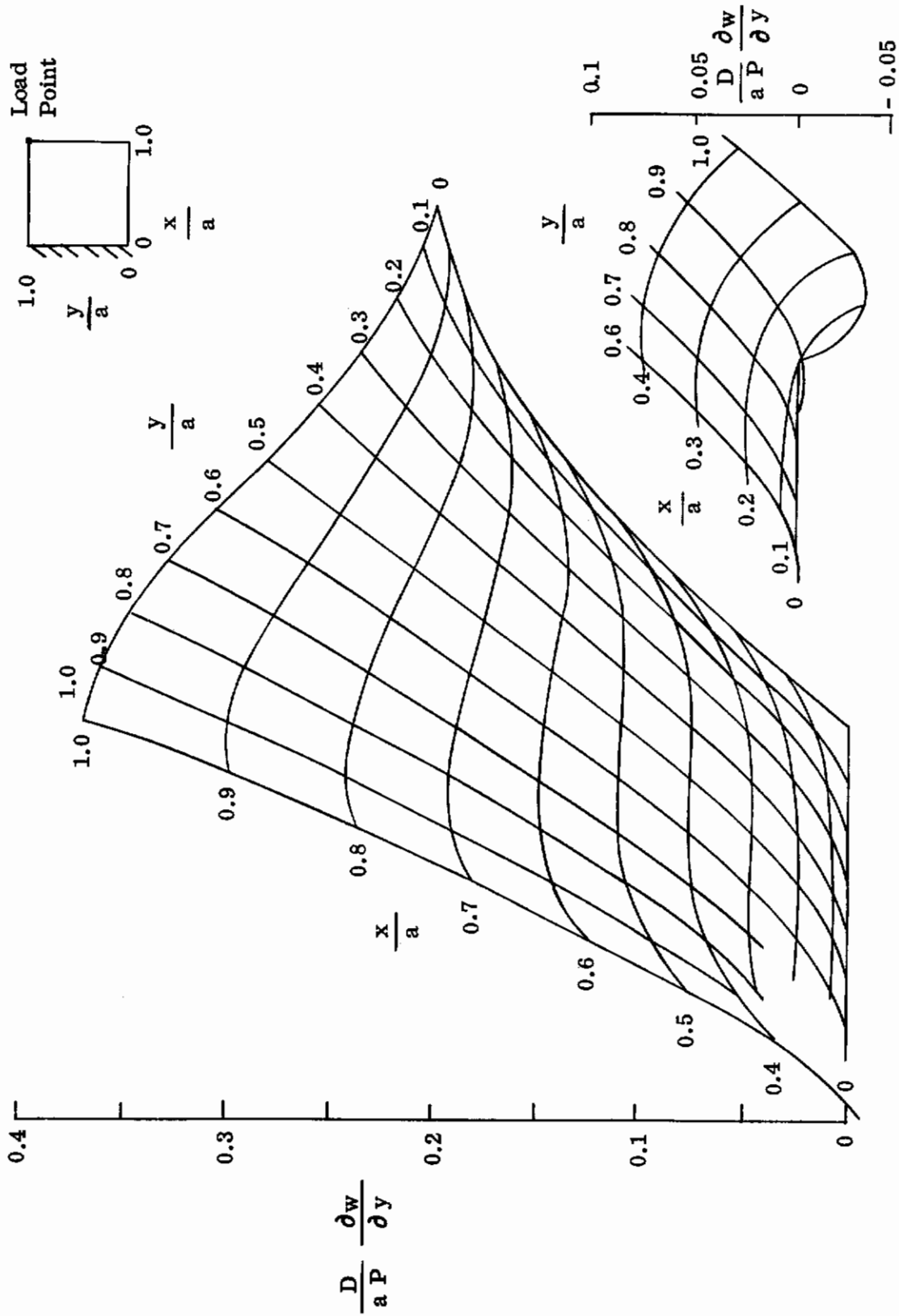
Figure 4.6. Square Cantilevered Plate — Analytically Derived Chordwise Slope
Influence Coefficients for Corner Point Load

Figure 4.7a for $\Delta \dfrac{\partial w}{\partial y} = 0.002$

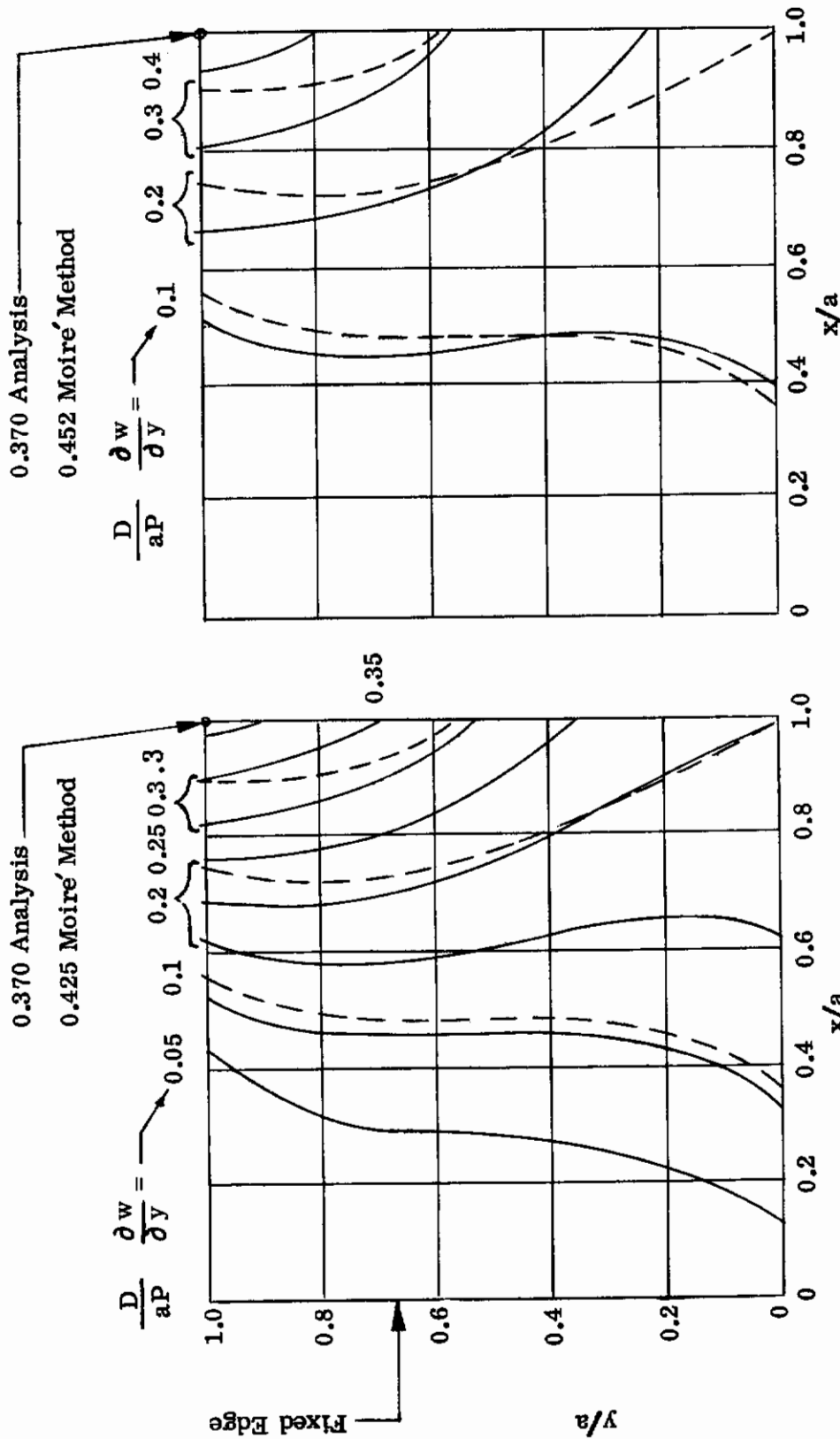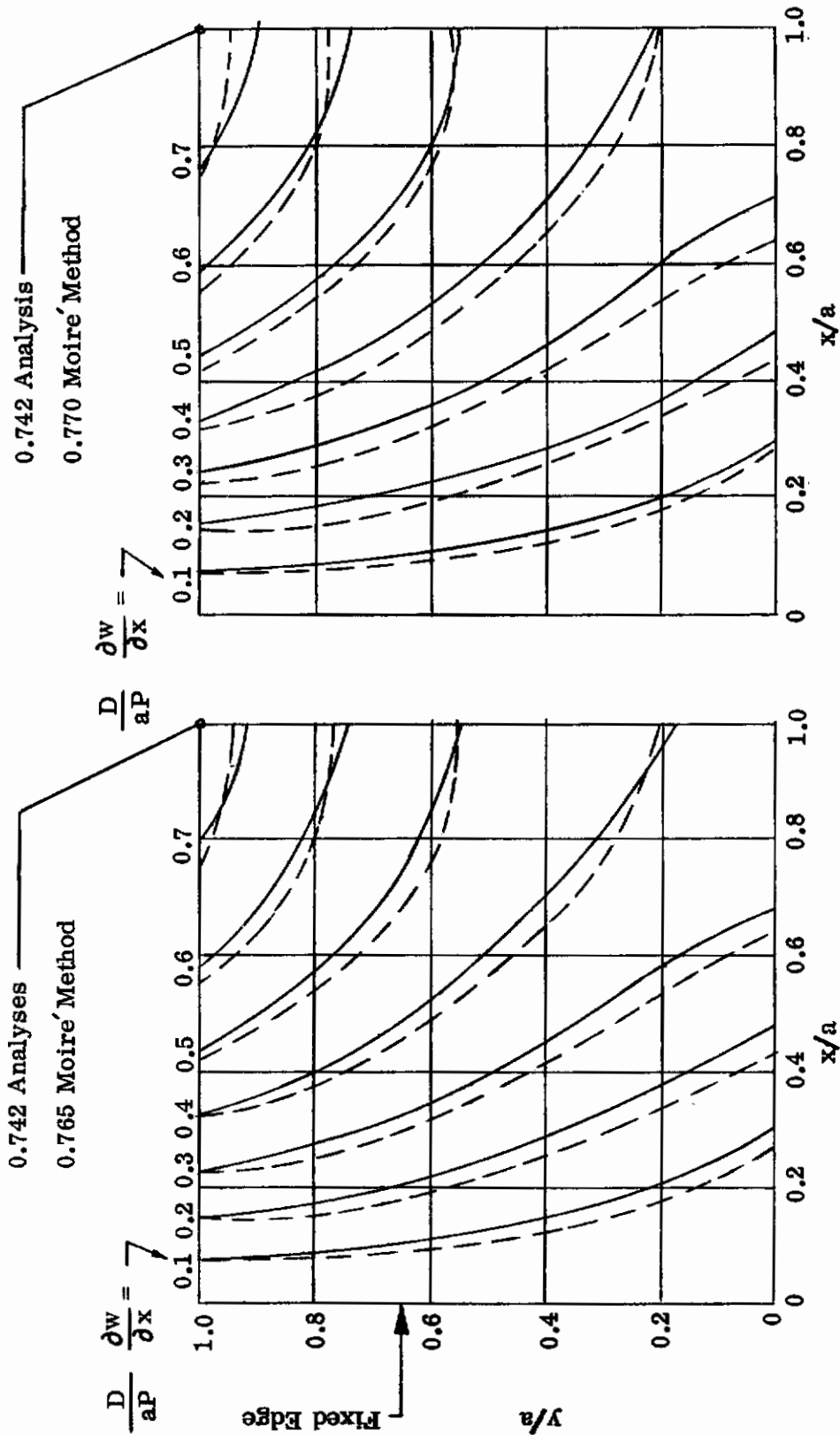Figure 4.7b for $\Delta \dfrac{\partial w}{\partial y} = 0.004$

Figure 4.7. Square Cantilevered Plate — Comparison of Analytical and Experimental
Chordwise Slope Influence Coefficients for Corner Point Load

37

Figure 4.8. Square Cantilevered Plate – Comparison of Analytical and Experimental Spanwise Slope Influence Coefficients for Corner Point Load

38

4.2   SWEPT WING

Photographs of the fringe patterns for the built-up swept wing model have been presented in Section 3.0. As in the case of the plate specimen, it is first necessary to reproduce the photographs as line drawings before comparisons with data obtained elsewhere can be accomplished. Interpretations of the more significant photographs are given in Figures 4.9 through 4.12.

Extensive deflection influence coefficient tests of this specimen were performed in a previous study (Reference 5) under identical support conditions. Numerous comparison analyses, employing various types of theoretical approaches, were also performed. It was found that although the shape of the deflected surface could be predicted quite well through use of certain of these approaches, there were fundamental differences in magnitude between the theoretical and test displacements. These differences were on the order of 20%. Thus, present comparisons are limited to the deflection influence coefficient test data.

By use of the deflection influence coefficients presented in References 5 and 6, it is possible to define the displacement of the tip chord due to a unit load at the tip corner point. This deflection profile is shown in Figure 4.13a. By numerical differentiation, the desired profile of the chordwise slope along the tip chord is obtained. This profile is shown in Figure 4.13b.

By operating on the results of Figures 4.9–4.12, another representation of the chordwise slope profile along the tip chord, that given by the Moire' fringes, is obtained. This reduction of the data from Figures 4.9 through 4.12, including a transformation into influence coefficient form (i.e., the values shown are for a unit load), is presented in Figure 4.14. Points delineate the location of fringe lines. The solid lines have been drawn as approximate boundaries on the Moire' fringe data.

Figure 4.9. Swept Wing – Contour Lines for Spanwise Slope Due to
Tip Corner Point Load of 89.9 Pounds

40

Figure 4.10. Swept Wing – Contour Lines for Spanwise Slope Due to
Tip Corner Point Load of 136.9 Pounds

41
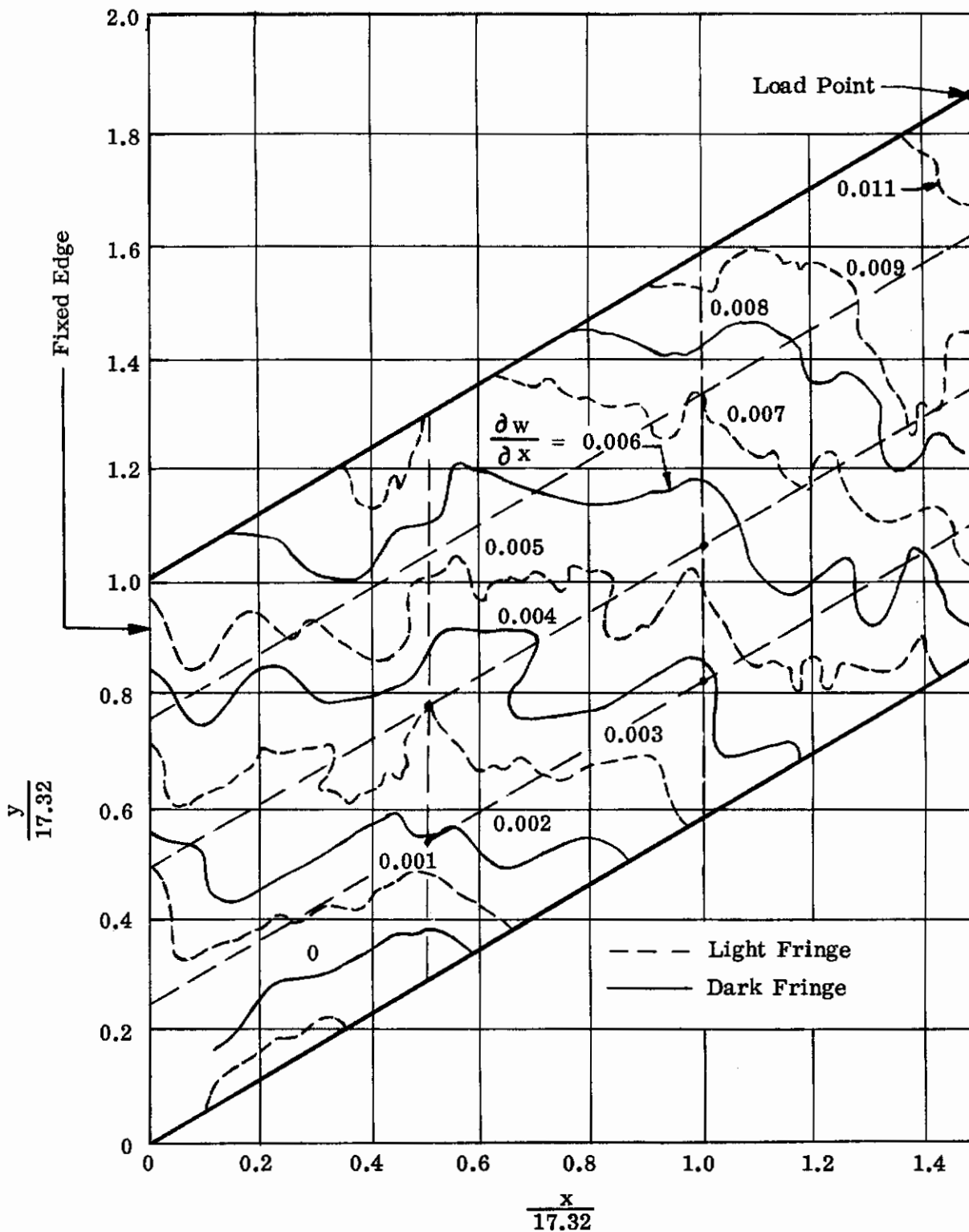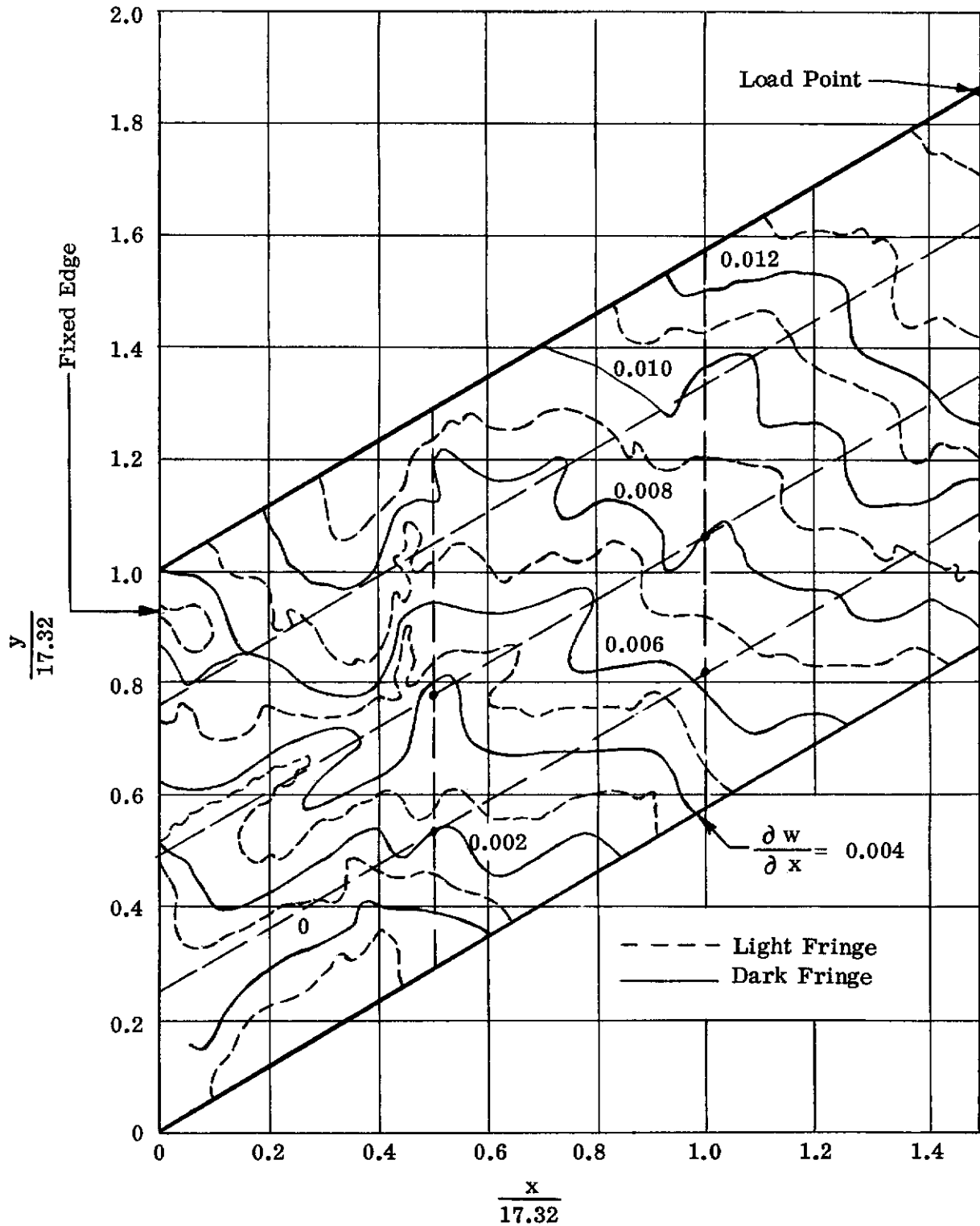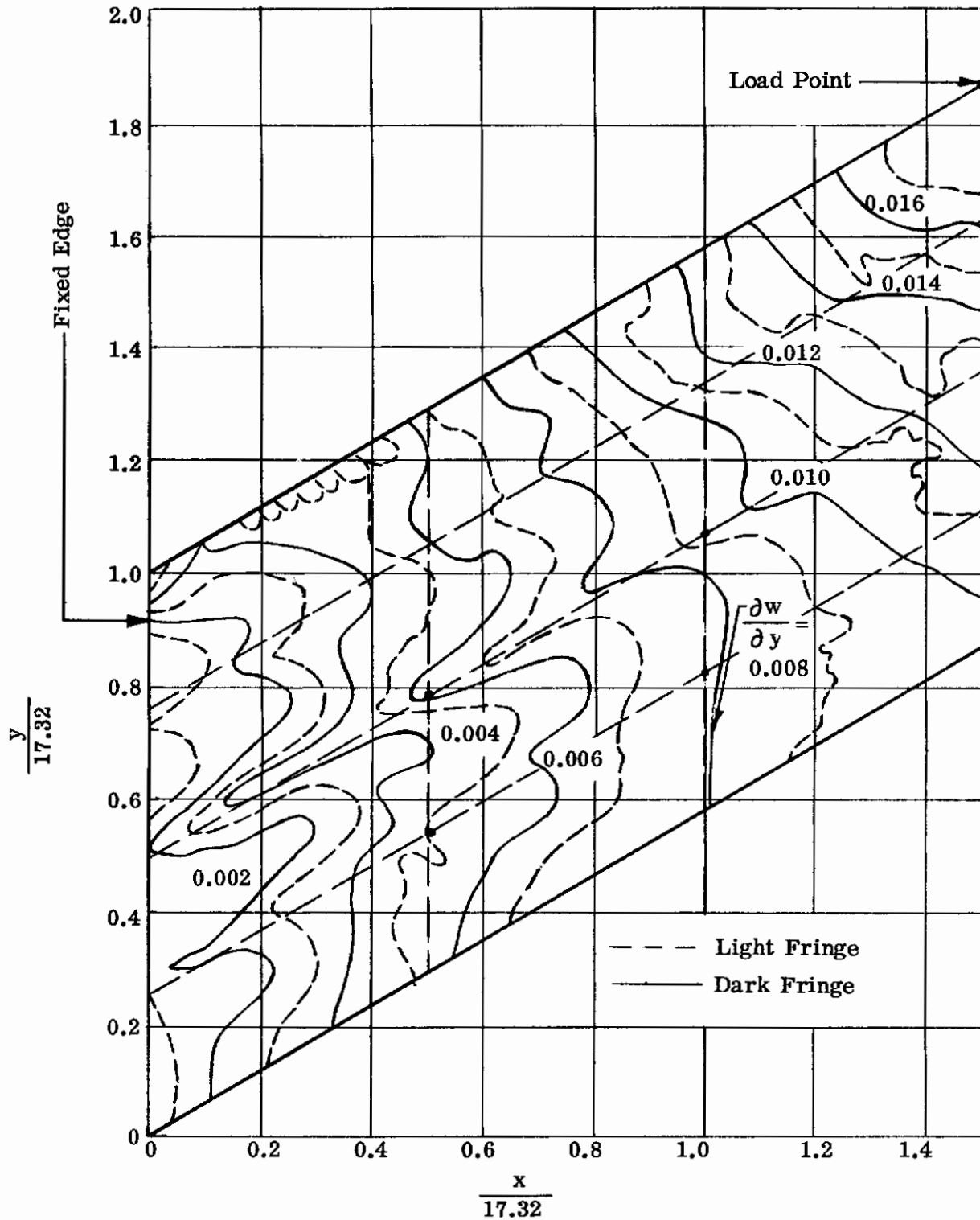
Figure 4.11. Swept Wing – Contour Lines for Chordwise Slope Due to
Tip Corner Point of 89.9 Pounds
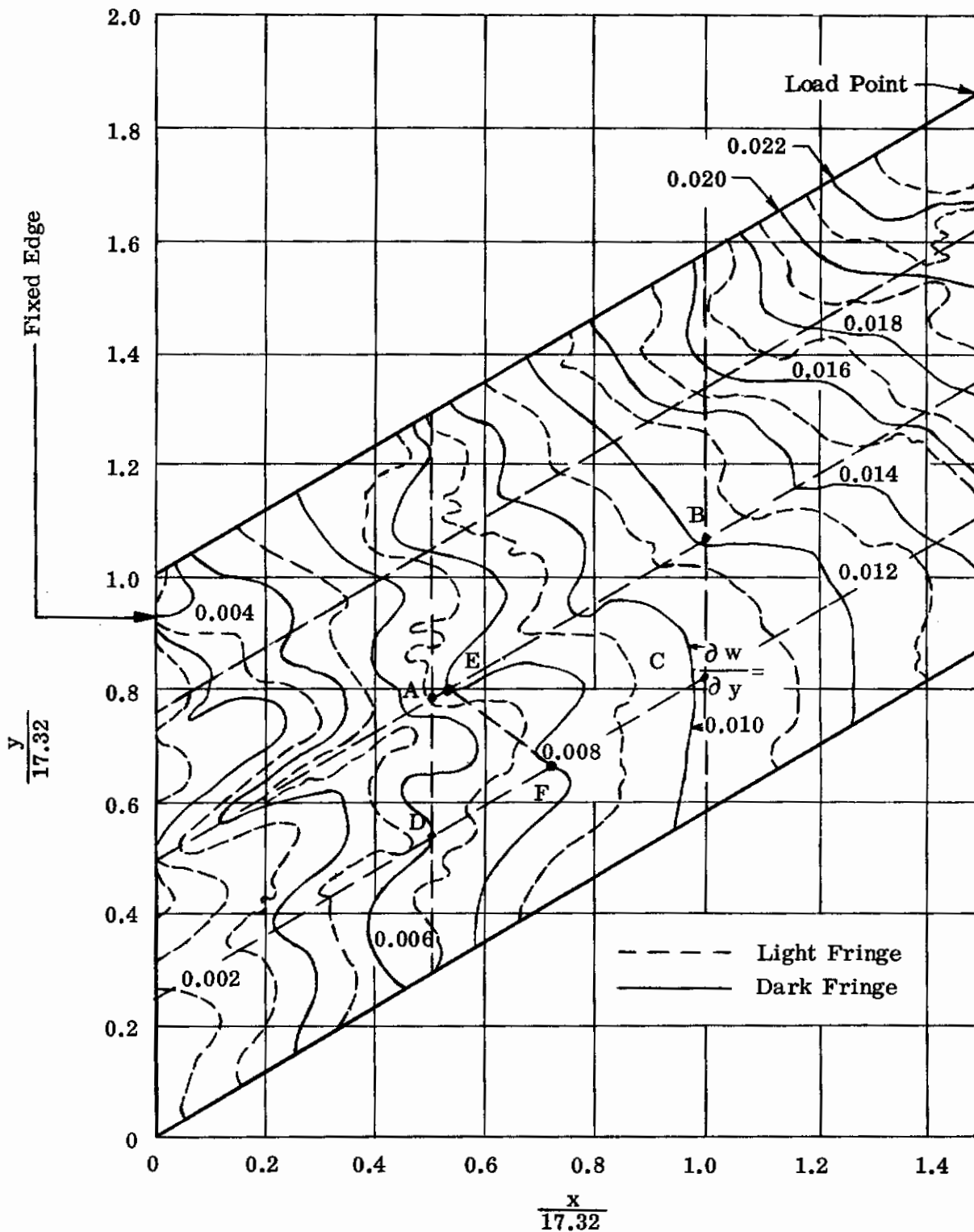
Figure 4.12. Swept Wing – Contour Lines for Chordwise Slope Due to
Tip Corner Point Load of 136.9 Pounds

43
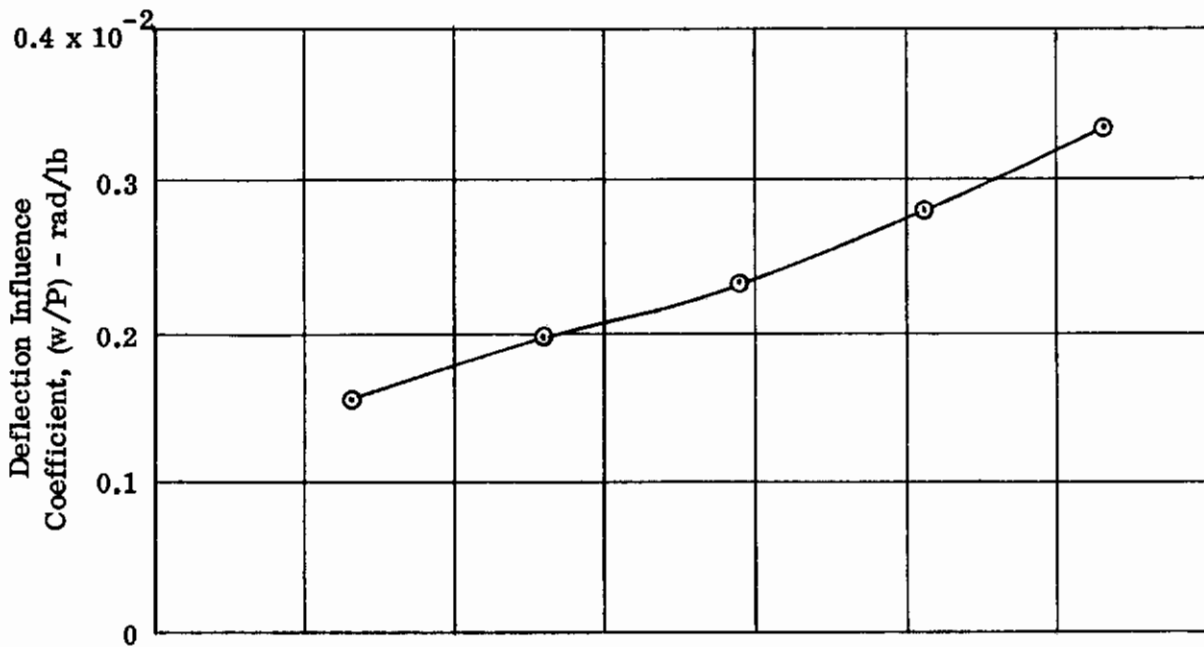
a. Deflection Influence Coefficients
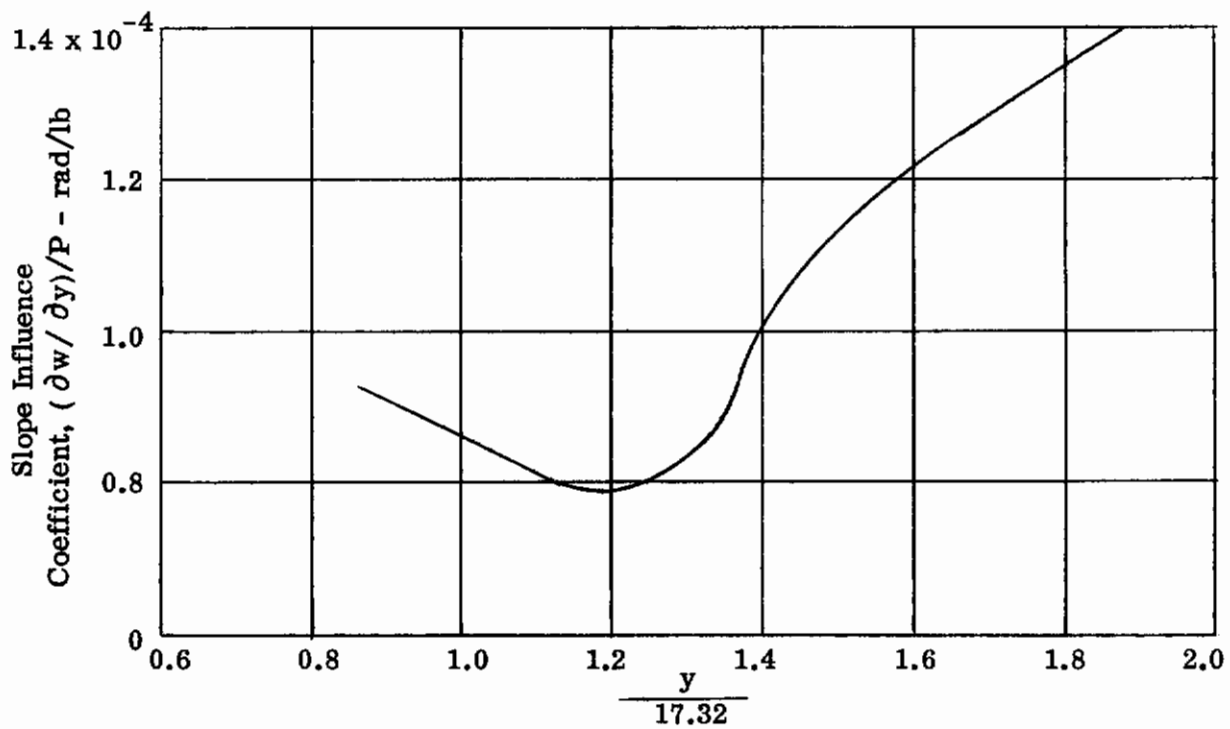
b. Slope Influence Coefficients

Figure 4.13. Swept Wing–Tip Chord Deflection and Slope Influence Coefficient
Test Data

44

Trailing Edge

2.2 x 10⁻⁴

□ Light Fringe 44.3 lb Load
■ Dark Fring 44.3
△ Light Fringe 89.9
▲ Dark Fringe 89.9
○ Light Fringe 136.9
● Dark Fringe 136.9

2.0

1.8

1.6

1.4

Slope Influence Coefficient $\frac{\partial w}{\partial y}$ /P — rad/lb

1.2

1.0

0.8

Results from
Figure 4.13 b

0.6

Leading Edge

0.4

0.2

0

0   0.8   1.0   1.2   1.4   1.6   1.8   2.0

$\frac{y}{17.32}$

Figure 4.14. Slope Influence Coefficients, $\frac{\partial w}{\partial y}$ /P for Swept
Wing Model Along Tip, ($\frac{x}{17.32}$ = 1.5)

45

The results interpreted from the deflection influence coefficient tests are given by the dashed line in Figure 4.14. Good agreement between both tests are indicated only at the leading edge. In general, the deflection test data are lower than the fringe data over most of the tip chord. It is of interest to note that the difference between both tests for values above $y/17.32 = 1.2$ is almost constant and approximately equal to 48%.

In reviewing this comparison, it must be emphasized that the values with which the Moire' fringe results are compared are developed in an approximate manner. from displacement test data and are not, therefore, a precise basis of comparison. Indeed, a number of a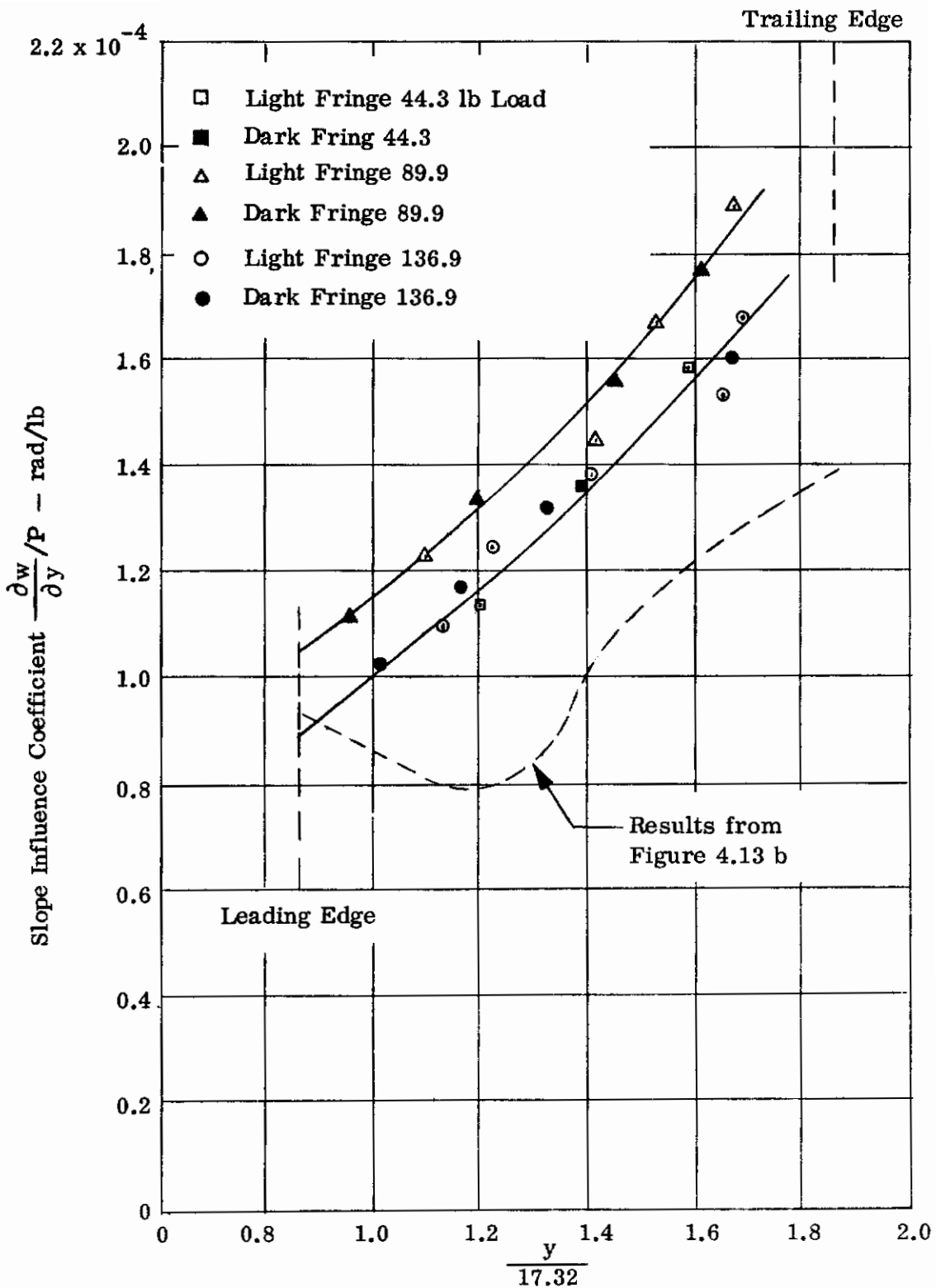pproximations reside in the development of the displacement influence coefficients from more fundamental test data (see Reference 5).

It should be noted that examination of the Moire' fringe patterns (Figures 3.7 and 3.8 and 4.9-4.12) discloses some interesting and significant aspects of the chordwise slope displacements in the regions between the spars and ribs. These regions are not dealt with in analysis methods nor in the conventional approach to displacement influence coefficient testing. Consider, for example, the region bounded by points A, B, C, D, on the surface of the swept wing as shown in Figure 4.12. These fringes represent chordwise slopes due to a 136.9 pound load at the tip corner point. From this figure it is seen that if the fringes in the region were to be defined by joining the spar fringe locations by straight lines, such as EF, (which is the procedure implied by measurements taken only at spar-rib intersection points) then there is a discrepancy with the actual fringe at the center of the region which, in general, indicates a lower slope. For example, the line EF joins the fringe for $\frac{\partial w}{\partial y} = 0.008$ at the spar lines. In the center of the panel, however, the fringes show a slope $\frac{\partial w}{\partial y} = 0.0065$.

46

SECTION 5.0

CONCLUSIONS AND RECOMMENDATIONS

The tests described in this report have shown that it is indeed feasible to obtain experimentally a complete picture of the slope deflections of a practical lifting surface structure. Bases for improvements which would be necessary for the attainment of required levels of accuracy and the improvements themselves are discussed in this section. Measurements taken during tests of a practical structure performed as part of the study were inconclusive with respect to the specific level of accuracy attained, due primarily to the approximate nature of the data with which the present results were compared. Thus, further evaluative test programs directed at improvement of Moire' techniques are desirable.

In discussing the means for improving the accuracy of the subject technique it is useful to consider separately its major component aspects; the ruled screen, the reflective surface, and the photographic technique. Improvement in photographic equipment, which represents another aspect of the technique, is regarded as a topic beyond the scope of the present study and is not discussed.

A.   PHOTOGRAPHIC TECHNIQUE

The double exposure technique proved adequate in the tests performed. The denser fringe patterns were difficult to evaluate, however, because of lack of sufficient contrast. Development of the photographic technique should therefore be directed toward means for improving contrast.

B.   RULED SCREEN

The construction of a surface for a ruled screen of the proportions required for a practical lifting surface would not be difficult. On the other hand, the definition of ruled lines on such a screen remains a problem. The use of adhesive backed sheets, as used in this study, proved satisfactory but nevertheless

possesses shortcomings which would no doubt be intensified for larger test arrangements. One promising technique would be to prepare large sections of accurate grid lines on stiff paper or cardboard which could be properly orientated on the screen.

An important item which influences the accuracy of the final results is the placement of the screen in its proper position relative to the specimen. For the relatively large test arrangement used in this study, it was found that small deviations in screen-to-surface parallelism introduces significant errors.

C. REFLECTIVE SURFACE

It has been demonstrated that it is feasible to make reflective the relatively large surfaces of practical airframe type structures. Of the various surface preparation techniques investigated, the attachment of a mirrored surface proved best. Vacuum metallized plastic sheet both in one large sheet and in patches, was employed. The effects on the results of surface imperfections (such as scratches, rivets or small surface waviness) are thereby eliminated.

Nevertheless, the imposition of reflective surfaces on test specimens represents the most important topic for future research. In particular, improvement of the technique for attaching mirrored sheets to structural surfaces with a minimum of waviness is most important.

A promising, but as yet unevaluated, method involves the application of liquid plastic to the test surface. After hardening, the plastic can be machined to a smooth surface and then vacuum metallized. In the case of a structure with an extensive surface area, this scheme might not be feasible since large vacuum metallizing facilities will be required. In such cases, it may be more practical to remove the hardened plastic in sections, vacuum metallize each section, and then cement each section back onto the surface.

Apart from the areas covered by A, B, and C, another area requiring additional study is concerned with the evaluation of the Moire' fringes when large deflections or curvatures are present. Under those circumstances, the distance

48

from the screen to the image on the specimen surface will not be a constant as was assumed in work performed in connection with this study.

In conclusion, it is to be emphasized that the Moire' fringe technique possesses an advantage over other experimental approaches to slope determinations in that it provides a survey of these slopes over the entire surface. Such comprehensive descriptions of structural behavior may be necessary if the current trend toward finer representations in aeroelastic analysis continues. As shown in Section 4.2, slope displacements in the regions of the surface between spars and ribs can be significantly different from slope displacements at these locations as predicted from measurements made only at the spar-rib intersection points.

The technique appears especially suited to experimental investigations at elevated temperatures, since no instrumentation need be located on or near the heated test specimen. Study and development would be required, however, of the temperature limitations of the various possible schemes for surface preparation.

The attention of this study has been limited to slope determinations. The Moire' fringe technique possesses additional advantages as a tool for stress analysis. These advantages have been exploited for plates in References 1 through 3. No work has as yet been published describing the application of the Moire' method to built-up structures with the objective of accomplishing stress determinations.

SECTION 6.0

REFERENCES

1. Ligtenberg, F.,"The Moire' Method – A New Experimental Method for Determination of Moments,"Proceedings of the Society for Experimental Stress Analysis, V. XII, No. 2, 1955.

2. Bradley, W. A.,"Laterally Loaded Thin Flat Plates,"Proceedings ASCE, Journal of the Engineering Mechanics Division, V. 85, No.EM 4, Oct. 1959, 77-107.

3. Palmer, P. J.,"The Bending Stresses in Cantilever Plates by Moire' Fringes," Aircraft Engineering, Dec. 1957.

4. Vinckier, A., and Dechoene, R.,'Use of the Moire' Effect to Measure Plastic Strains,'Transactions ASME, Vol. 82, No. 2, Series D, 1960.

5. Rattinger, I., and Gallagher, R. H., Supersonic Aeroelastic Effects on Static Stability and Control - Part II, "Structures", WADC TR 58-95, April 1960.

6. Gallagher, R. H., and Rattinger, I., The Deformational Behavior of Low Aspect Ratio Multi-Web Wings, Part I - "Experimental Data," Aeronautical Quarterly, Nov. 1961.

7. Batt, J. R., and Gallagher, R. H., Nonlinear Thermoelastic Effects on Hypersonic Stability and Control, Part II - "Analytical and Experimental Static Aerothermoelasticity", FDL-TDR-64-16, January 1964.